A study of the capability of Flamelet-based Combustion Model for the Gas-phase Combustion of a Grate-firing Biomass Furnace

By

A H M Nazmush Sakib

A Thesis submitted to the Faculty of Graduate Studies of

The University of Manitoba

In partial fulfillment of the requirements of the degree of

Master of Science

Department of Mechanical Engineering

University of Manitoba

Winnipeg

ABSTRACT

Canada's new short-term greenhouse gas (GHG) emissions target, resulting from the 2015 Paris Agreement, has led the energy production industry to adopt more carbon-neutral fuels, including biomass. Hence, the development of biomass combustion technology has recently gained more attention owing to its capability to burn a wide range of biomass fuels. Computer simulation of biomass furnaces is a very important step towards improving the combustion performance and emissions of these power generation systems. Combustion models play a key role in the reliability of the numerical simulation of the gas-phase combustion of biomass combustion systems. The aim of the present numerical study is to evaluate the prediction capability of flamelet-based partially premixed combustion models in simulating the gas-phase combustion process of a grate-firing biomass furnace. Additionally, the effects of the adopted premixed models (i.e., extended coherent flame model and C-equation based model) and non-premixed models (i.e., steady diffusion flamelet (SFM) and unsteady diffusion flamelet (UFM)) on the overall prediction of the partially premixed model are assessed. The predicted temperature field and species concentrations are compared with published experimental measurements and also with published numerical simulations which use other combustion models (i.e., EDC/Flamelet hybrid model, SFM and UFM). The results of this study reveal that except for the slow-forming and chemically dominated species, partially premixed combustion models (both extended coherent flame model/SFM and C-equation/SFM-based partially premixed model) are capable of reproducing the experimental temperature and major species with reasonable accuracy and low computational expense. C-equation/UFM-based partially premixed model is found to be the most optimum combination amongst all examined partially premixed models for overcoming the deficiency faced while predicting the slow-forming species.

ACKNOWLEDGEMENTS

I would like to begin by expressing my utmost gratitude to my research advisor Dr. Madjid Birouk for providing me with this wonderful opportunity to work under his supervision and for his continuous support and encouragement throughout the process.

I would like to thank Dr. Vijay Chatoorgoon and Dr. Qiang Zhang for serving on my thesis committee and taking the time to provide valuable feedback on my thesis. Also, I would like to thank Dr. Mohammadreza Farokhi for sharing his experience and knowledge during the investigation and my fellow colleagues from the Energy and Combustion Laboratory at the University of Manitoba for their help and fruitful discussion.

I would like to acknowledge the financial support received from the Natural Sciences and Engineering Council of Canada (NSERC) and the industrial partner, SteelTech Inc., along with the Faculty of Graduate studies at the University of Manitoba.

I would like to thank my parents, especially my father, for being the inspiration of my life and for always being there for me without any doubt. His journey has always given me the strength to move forward and reach for the goals that are beyond my forte.

Finally, I would like to thank my wife, Nasiba Maruf Ahmed, for being my best friend and my support system. I would like to dedicate my thesis to my son Avan.

TABLE OF CONTENTS

LIST OF FIGURES

LIST OF TABLES

LIST OF EQUATIONS

NOMENCLATURE

Symbols:

a	Absorption coefficient
σ_s	Scattering coefficient
C	Linear-anisotropic phase function coefficient
G	Incident radiation
n	Refractive index of the medium
T	Local temperature
S_h	Radiation heat flux's effect
q_r	Radiation flux
$a_{\varepsilon,i}(T)$	Emissivity weighting factor of the i^{th} fictitious gray gas as a function of temperature
s	Path length
P	Sum of the partial pressures of all absorbing gases
k_i	Absorption coefficient of the i^{th} gray gas
m_p	Particle's mass, kg
K_c	Mass transfer coefficient, m s^{-1}
A_p	Particle's surface area, m^2
$Y_{w,s}$	Mass fractions of vapor at the surface of the particle
Y_w	Mass fractions of vapor at bulk gas
C_p	Latent heat of water
T_p	Particle's temperature, K
h	Convective heat transfer coefficient, W m^{-2} K^{-1}

h_{fg}	Latent heat of water, J kg^{-1}
K_c	Mass transfer coefficient, m s^{-1}
$D_{w,m}$	Diffusion coefficient of vapor in bulk gas, m^2 s^{-1}
Re_d	Particle's Reynolds number
Sc	Schmidt number
d_p	Particle's diameter
k	Turbulent Kinetic Energy, m^2 s^{-2} – thermal conductivity, W m^{-1} k^{-1}
Pr	Prandtl number
E	Model constant, 20 kJ/mol
A	Model constant, 1.5e-2 s^{-1}
$Y_{v,0}$	Initial mass fractions of moisture in the particle
$Y_{w,0}$	Initial volatile in the particle
Y_{ox}	Mass fraction of the oxidizer
$m_{p,0}$	Initial mass of the particle
MW_{ox}	Molecular weight of the oxidizer
R_{dif}	Diffusion rates of char combustion
R_{kin}	Kinetic rates of char combustion
$\bar{c}$	Mean reaction progress variable
f	Mixture fraction
Sc_t	Turbulent Schmidt number
P_1	Source due to turbulence interaction
P_2	Source due to dilatation in the flame
P_3	Source due to expansion of burned gas

P_4	Source due to normal propagation
D	Dissipation of flame area
∇	Vector differential operator
σ	Stefan-Boltzmann constant, kg s^{-3} K^{-4}
ε	Turbulent dissipation rate, m^2 s^{-3}- emissivity
ρ	Density, kg m^{-3}
θ	Radiation temperature, K
$\overline{\emptyset}$	Density-weighted mean scalars
$\emptyset_b$	Burnt scalar
$\emptyset_u$	Unburnt scalar
μ_t	Turbulent viscosity
Σ	Mean flame area density

Acronyms:

CFD	Computational fluid dynamics
DPM	Discrete phase model
EDC	Eddy dissipation concept
EDM	Eddy dissipation model
FRK	Finite-rate kinetic
MILD	Moderate to intense low-oxygen dilution
PSR	Perfectly stirred reactor
RANS	Reynolds Averaged Navier-Stokes
RKE	Realizable $k-\varepsilon$

RNG	Renormalization group
RSM	Reynolds stress model
SFM	Steady flamelet model
UFM	Unsteady flamelet model
WSGG	Weighted-sum-of-gray-gas
RSM	Reynolds Stress Model
DES	Detached Eddy Simulation
LES	Large Eddy Simulation

Chapter 1 INTRODUCTION

1.1 Background

Petroleum products (e.g., fossil fuel variants) are still responsible for producing around 84% of the total global energy demand in transportation, industrial and residential combustion plants, while only 5% of this enormous demand relies upon renewable energy resources (e.g., biomass, hydro, wind and solar energy resources) [1],[2]. Due to this high consumption rate and a limited reserve of petroleum products, the energy industry will face excessive production costs that will eventually lead to the exhaustion of their reserve [3], [4]. The limitation of petroleum and other fossil fuels coupled with increasing global warming has shifted the focus to renewable energy resources like biomass [3], [5], [6]. Organic materials that originate from the plant are the main source of biomass. Solar energy is absorbed by biomass cells through photosynthesis that can be used as a source of inexhaustible renewable energy originating from nonedible parts of plants [7]. Moreover, the amount of emitted CO_2 in the environment while producing energy is equal to the amount of absorbed CO_2 during photosynthesis, which makes biomass carbon-neutral [8]. Research on carbon-neutral fuel-based energy production (e.g. biomass) has been fuelled by the growing demand for renewable energy sources [6], [9].

Biochemical and thermochemical are considered two major technologies for converting and burning biomass into useful energy resources, and both technologies either directly convert biomass to heat or to an energy carrier [7]. Bacteria are used for changing biomass into an energy carrier in the biochemical conversion method where organic matter is dissolved by bacteria and high-methane content gases consisting of methanol and ethanol are produced [7]. On the contrary, the thermochemical method involves either direct energy carrier extraction from biomass residue using heat or direct conversion of biomass to energy through combustion [7].

For the production of biomass-based power and heat, direct combustion in a furnace is the most widely established technology [5], [6], [10]. Biomass combustion devices are expected to emit lesser compared to fossil fuel-based combustion technologies as they belong to renewable energy sources. Incomplete combustion is the reason behind the emission of harmful pollutants from the burning of biomass, and this is a more common phenomenon for small-scale biomass furnaces because of poor air/fuel mixing and shorter residence time [6]. Several factors, such as fuel type, ash properties, moisture content and heating value, can have an influence on the design of commercial furnaces [7]. Pulverized bed or suspension furnaces, fluidized bed furnaces and fixed bed or grate-firing furnaces are the most common classifications of biomass furnaces [7]. Pulverized beds are designed to accommodate coal combustion. These furnaces are used for the combustion of coal-pulverized raw biomass, and biomass particles with lower moisture and higher volatility are preferred for this type of furnace [7], [11]. In the case of fluidized bed systems, solid biomass particles are mixed with an inert material and suspended in a partial volume of the furnace with injected air at high velocity, and the huge quantity of inactive material inside this type of furnace causes low ignition temperature (800-950°C) [7].

On the other hand, grate-firing biomass furnaces are capable of dealing with an extensive range of biomass fuel types, sizes and moisture content. For these reasons, the prevalence of industrial grate-firing biomass furnaces has increased in recent times more than ever before [6], [12]. However, grate-firing biomass furnaces still have relatively low thermal efficiency and produce undesirable pollutants. Therefore, several researches have been conducted using both experimental and computational in order to maximize the performance of this technology and, at the same time, minimize pollutant emissions [13]. Experimental methods involve the collection of experimental data on velocity and temperature fields as well as gaseous emissions composition [14].

Experimental measurements can provide invaluable insights into the phenomena and, at the same time, provide input data for computational simulation validation [15]. However, experimental studies are very limited due chiefly to high costs and technical challenges [16]. On the contrary, by introducing a virtual view of the flow and chemical kinetics interaction in a computational domain, a CFD framework can help achieve a reasonable understanding of the biomass combustion process with a much cheaper cost than physical testing [16]. The numerical modelling steps can be divided into two main sections (i.e., bed and gas-phase combustion modelling), and the reliability of the CFD predictions is highly dependent on the accuracy of these two models [17]. Although these two models are closely co-dependant, most often, they are modelled separately.

1.2 Combustion Modelling of a Grate-firing Biomass Furnace

Combustion occurring in a grate-firing biomass furnace undergoes two successive phases; that is, the conversion of solid fuel on a fixed or moving grate in the presence of primary airflow (usually coming from underneath the fuel layer) into volatile gases [18] and the gas-phase combustion occurring in the freeboard space, also known as over-fire biomass combustion [16]. In accordance with their nature, these two successive phases (i.e., conversion of solid fuel and gas-phase combustion) have been described as heterogeneous [18] and pure homogeneous [12] processes, respectively. After being modelled separately, they are required to be connected through an interface for transferring the information. Figure 1 shows the connection between the freeboard and the bed in a numerical simulation. A brief description of bed modelling and gas-phase combustion in the freeboard of a grate-firing biomass furnace is given below.

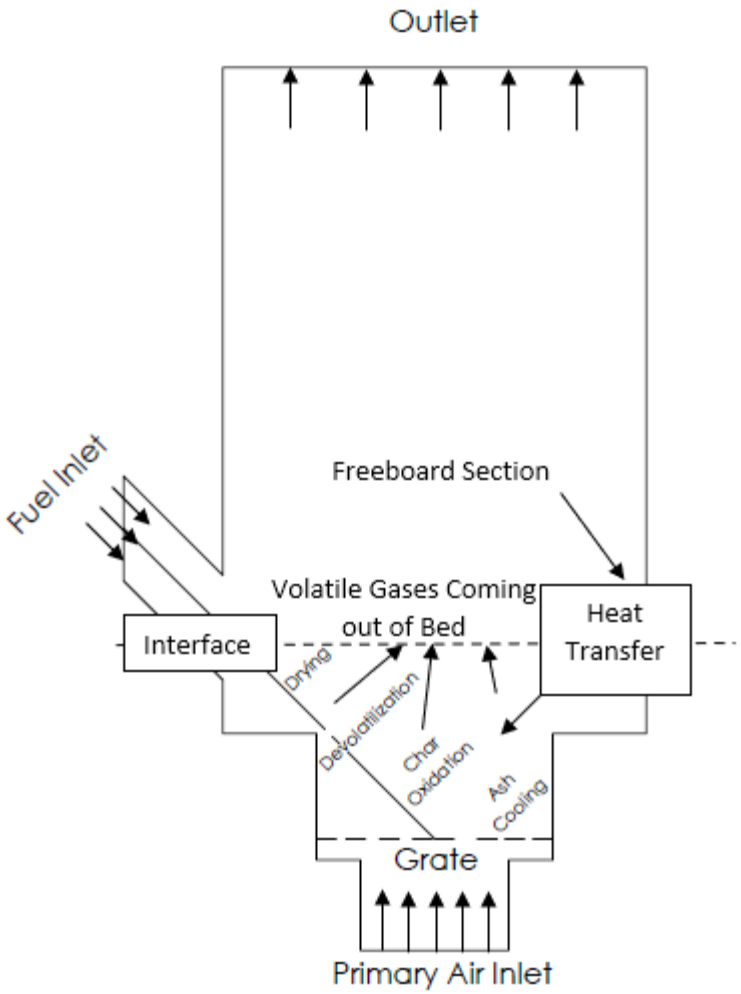

Figure 1. Schematic representation of biomass conversion in fuel bed and gas-phase combustion in freeboard section (Adapted from Refs. [7], [19])

1.2.1 Bed modelling

Conversion of solid fuels in the bed section takes place in the presence of air. In the case of grate-firing biomass furnaces, this air comes from beneath the bed/grate, and this type of fuel bed is termed the packed bed. An integral bed model is typically used to model biomass conversion in grate-firing furnaces due to the solid fuel decomposition on the grate, and it provides the necessary inlet boundary conditions used for the simulation of the gas-phase combustion occurring in the freeboard space [13]. Species mass fractions and temperature profiles at the fuel bed inlet

boundary are provided by simple bed models. These profiles can be obtained using the experimental measurements of temperature and species concentration above the bed or calculated on the basis of mass and energy conservation between the inlet (i.e., primary air and raw biomass particles) and outlet (i.e., released volatile gases) of the bed [20]–[23]. Separate sub-models are used by complex bed models in order to compute each conversion process to provide local temperature and mass fractions of released species [24], [25]. These conversions (i.e., physical and chemical) processes of solid fuel can be divided into three major phases (Drying, Devolatilization and Char oxidation) [18].

1.2.1.1 Drying

Vaporization of water content from the solid fuel is referred to as the drying phase, and the fuel conversion procedure commences with the initiation of the drying phase. The drying phase starts promptly after the fuel is fed into the furnace [26]. Fuel heats up with the absorption of heat from furnace walls and surrounding gases through convection and radiation, and the fuel moisture dries up as soon as the inner temperature of biomass reaches 100°C, which results in the reduction of inner temperature. The drying phase is an integral part of achieving efficient combustion. Combustion is not possible with a moisture content of 60% or more because the required amount of energy for vaporization of this amount of moisture exceeds the produced energy by the biomass fuel [7].

1.2.1.2 Devolatilization

The decomposition of solid fuels under thermal influence is called devolatilization. This procedure is also termed pyrolysis, and thermal decomposition and volatiles are formed in this process [26]. Thermal cracking reactions, along with heat and mass transfer reactions, are involved in this process which results in the release of permanent light gases (e.g. CO, CO_2,

H_2O, H_2, NH_3, CH_4), tar and char [27]. Released volatile gases leave the bed through the pores in the fuel bed surface and take part in the gas-phase combustion in the presence of oxidizers, and heat released in this phase influences both drying and de-volatilization processes [7]. The normal temperature range of a de-volatilization zone is between 200°C and 500°C[7]. After the release of volatiles, the fuel bed is left with only char and ash. The quantity of derived char increases with increasing the devolatilization temperature and rate [26]. Devolatilization is a heterogenous process, and simple models using single or multiple-step reactions are used to describe this process [18].

1.2.1.3 Char Oxidation/Combustion

This step involves the combustion of char (i.e., the remainder of carbon particles from the devolatilization step) in the presence of an oxidizer. The flow of released gases from the bed in the de-volatilization area makes it harder for the oxygen to come in contact with the surface of the particles, which prevents its reaction with the remainder of solid carbon in the particles. Although at the end of the devolatilization process, the reaction of oxygen with char particles are attainable [26]. The density of char is largely dependent on the final temperature and heating rates. Char concentration increases with slower heating rates as it gives more time for char production from chemical-bound conversion [26]. The combustion rate of char depends on the exposed surface, available oxygen and surrounding temperature because it is a diffusion-monitored procedure and this combustion releases mainly CO and CO_2 as emission gases [7].

1.2.2 Over-fire/Gas-phase combustion modelling

The volume of a grate-firing furnace situated above the bed section is known as freeboard space, and combustion occurring in this space is also called over-fire or gas-phase combustion [16]. Fuel inlet conditions are provided by the bed into the freeboard [16], and additional inlet air is

introduced into the freeboard in the form of secondary air and in some cases also, tertiary air [16]. Emitted volatile gases from the bed section and fresh air from the injected additional airflow (secondary or secondary and tertiary) participate in the mixing procedure in the freeboard section [16]. Thermal energy produced in this section reciprocally aids the drying and devolatilization procedure in the bed section, and the additional energy is harnessed through the heat exchanger that is situated in the path of flue gas emission. It is notable to mention that CFD studies of the gas-phase combustion in the freeboard require a variety of sub-models (including radiation, turbulence, combustion models, and chemical mechanisms) to describe the velocity flow field, heat and mass transfer, and interaction between chemistry and turbulent flow and the CFD predictions of the combustion of volatile gases in the freeboard section depend significantly on the reliability of the adopted sub-models [17].

1.3 Motivations

In the numerical simulation of the gas-phase combustion of a grate-firing biomass furnace, combustion models are responsible for modelling chemistry and its interaction with the flowfield. The computational cost largely depends upon the adopted combustion model and its ability to incorporate detailed chemical kinetic mechanisms.

Classical species transport combustion models (e.g., finite kinetic/eddy dissipation model (FKR/EDM) [28], eddy dissipation concept (EDC) [29]) have always been the center of attention when conducting numerical studies of biomass combustion in furnaces in spite of their inability to incorporate detailed chemical kinetic mechanisms without compromising the computational cost. Therefore, it has not been possible to conduct extensive studies on the emission of slow-forming species like CO, as the prediction accuracy of slow forming species largely depends upon the adaptability of detailed chemical kinetic mechanisms [30], [31].

To solve this issue, new mixture fraction-based (i.e., flamelet-based) models have been proposed as an alternative to the classical approaches [32] in order to account for the turbulent non-premixed combustion in industrial furnaces. Non-premixed mixture fraction-based models, which are termed as Steady flamelet model (SFM) and Unsteady flamelet model (UFM), were initially proposed by Peters [33], and they are capable of incorporating detailed chemical kinetic mechanisms without compromising the computational cost. A few studies have adopted these models, and the results indicated their incapability of properly simulating a grate-firing furnace [13], [17], [32]. Referring to the various degrees of local mixing between the oxidizer and fuel in grate-firing biomass furnaces, some researchers have termed the gas phase combustion as partially premixed combustion [33]–[35] and this phenomenon results in the co-existence of different combustion regimes (i.e., non-premixed, premixed and partially premixed). The literature adopted mixture fraction-based models are purely non-premixed models, and this could be a contributing factor to their limitations. Thus, in order to overcome these limitations, further research is required to evaluate alternative models, such as mixture fraction-based models (i.e., partially premixed combustion models).

1.4 Objectives

This study aims to conduct a comprehensive study on the applicability of flamelet-based combustion models for reliably simulating the gas-phase combustion of a grate-firing biomass furnace. The objectives of this study are as follows:

1. Examine the applicability of flamelet-based (mixture fraction-based) partially premixed combustion models for simulating the gas-phase combustion of a grate-firing biomass furnace.

2. Examine the effect of different non-premixed models (i.e., SFM and UFM) and premixed models (i.e., extended coherent flame model and C Equation-based model) on the prediction ability of partially premixed combustion model and determine the most optimum combination for the partially premixed model.
3. Compare the predictions of partially premixed combustion models with non-premixed models and determine the reason behind the limitations of non-premixed models.
4. Evaluate the capability of partially premixed combustion models against those more complex ones, such as the EDC-Flamelet combustion model.

1.5 Outline of the thesis

This thesis is an accumulation of six different chapters. 0 is an introduction to the subject being studied in this thesis. A literature review focusing on biomass combustion modelling is reported in Chapter 2. Chapter 3 describes the methodology, including a descriptive illustration of different sub-models adopted for conducting the simulations. Chapter 4 documents all the boundary conditions for running the simulations. Chapter 5 presents the results and their discussion. Finally, concluding remarks and some recommendations for future work are summarized in Chapter 6. Some additional details are presented in the Appendices at the end of the thesis.

Chapter 2 LITERATURE REVIEW

2.1 Introduction

Different studies that have been conducted on the gas-phase combustion of grate-firing biomass furnaces were mostly focused on the improvement of the mixing process and increment of the residence time of the volatile gases inside the combustion chamber. For this, various improvements and modifications of the furnace geometry have been proposed and studied numerically to avoid the enormous cost required for experimental investigations [16]. To be able to completely rely on these numerical methods, developing and providing a reliable CFD platform has always been the main focus of published research. To this end, over the years, different sub-models have been proposed and tested by researchers and the reliability of numerical results was found to strongly depend on the accuracy of these sub-models (e.g., turbulent sub-model, chemical kinetic reaction mechanism, and flow/chemistry interaction sub-model known as combustion models) [17]. A review of these sub-models is presented below.

2.3 Overview of different Sub-Models

Sub-models adopted while numerically modelling the gas-phase combustion of a grate-firing biomass furnace can be categorized into three main classes: turbulent models, radiation models and combustion models. Turbulence has a significant impact on gas-phase combustion, and the presence of various degrees of turbulence inside a grate-firing biomass furnace and their effect on the mixing process of the volatile gases contributing to the overall combustion is taken into account by the adopted turbulent model [33]–[35]. Radiation models are responsible for predicting temperature distribution inside a grate furnace, and this is crucial for determining the chemical kinetic rates of the volatile gas-air mixture in the freeboard space above the bed. Furthermore, the

heat transfer from hot furnace walls by the radiation process, which has an influence on the devolatilization and combustion of fuel particles in the fuel bed, is also addressed by a radiation model [36]. Finally, combustion models combine all the information from the above-mentioned sub-models and is responsible for the coupling between the chemical mechanisms and flowfield [37]–[39]. So thermal radiation, turbulent field characteristics, species of oxidizer, combustibles, and different chemical kinetic mechanisms are defined by these sub-models, all of which affect the overall predictions of combustion characteristics and pollutants emission. As a result, the degree of simplification and capability of the turbulence and combustion model, along with kinetic reaction mechanisms and radiation model, are the main factors that have an influence on the prediction reliability of the over-fire combustion model [16].

2.3.1 Turbulence Models

Among all turbulence models (i.e., RANS-based, LES, DES and DNS), RANS-based turbulent models are more widely used for describing the turbulent flow field inside an industrial furnace. In the context of industrial implications, these turbulent models can be classified into two major categories:

Two-Equation Models ($k-\varepsilon$ models): Two-equation $k-\varepsilon$ models are based on the hypothesis of Boussinesq [40] for relating the Reynolds stresses to the mean velocity gradients of RANS equations. In spite of this model's limitations while predicting a flow field with a large adverse pressure gradient, its popularity in industrial flow and heat transfer simulations is unmatched due to its robustness, economy and reasonable accuracy for a wide range of turbulent flows. The two equations of this model are responsible for the calculation of the historical effects of convection and diffusion of turbulent energy [41].

The transported variables are $\boldsymbol{k}$ and $\boldsymbol{\varepsilon}$ (turbulent kinetic energy and turbulent dissipation, respectively).

Other Models: Reynold stress model (RSM), Large eddy simulation (LES) and Direct numerical simulation (DNS) can all be used in the simulation of industrial furnaces. However, the literature showed that only the RSM model had been tested for simulating biomass furnaces [42], [43], [44]. The main benefit of using the RSM model over the other two models (LES and DNS) is that it is simple [7]. On the contrary, LES and DNS are complex models and require solving all turbulence scales.

Turbulence in an industrial biomass furnace is usually modelled using the standard (STD) $k-\varepsilon$ model [41], [45], renormalization group (RNG) $k-\varepsilon$ model [46] and realizable (RKE) $k-\varepsilon$ model [47] which also known as two-equations model. These models not only follow different calculation procedure for determining turbulence viscosity and turbulent Prandtl number but also use different transport equations for calculating turbulent dissipation rate [41]. For modelling turbulence in industrial biomass furnaces, the STD model has been widely used [24], [25]. While performing a comprehensive CFD modelling of a domestic biomass stove, the STD $k-\varepsilon$ turbulence model along with transport equations of mixture fraction for the gas-phase combustion in the freeboard was adopted by Tabet et al. [48]. A review study was conducted by Chaney et al. [21] for examining the role of STD $k-\varepsilon$ model in a CFD modeling of small-scale grate firing biomass furnace for the optimization of combustion performance and NO_x emission. According to these studies, a reasonable prediction of velocity, species and temperature fields were made by STD $k-\varepsilon$ model at different inlet airflow conditions.

Collazo et al. [49] used the RKE turbulence model for the simulation of a domestic pellet boiler and found that, when compared to experimental measurements, it is capable of predicting temperatures and species profiles more satisfactorily. A three-dimensional (3D) CFD simulation of a small-scale biomass furnace was conducted by Buchmayr et al. [13] using the RKE turbulence model for gas-phase combustion and reported an acceptable prediction of temperature and gas emissions in comparison with experiments.

In a different study, both STD $k-\varepsilon$ and the Reynolds stress model (RSM) were tested by Fletcher et al. [42], [43] for predicting flow entrainment in a biomass gasifier under isothermal (cold) and flame conditions. According to their reports, the predictions (i.e., temperature, gas concentrations and velocity field) of the reacting flow field are less sensitive to the adopted turbulence model in comparison with the predictions of the cold flow case [42]. Changes in the density and hence velocity within the gasifier caused by combustion were identified as the cause for these differences. Knaus et al. [44] performed a gas-phase simulation in the freeboard of a small-scale 15KW wood heater and examined different turbulence models. In this simulation low Reynolds number and STD $k-\varepsilon$ models along with RSM turbulence model were tested under cold flow and combustion conditions. They reported that different turbulence models predicted the flowfield differently, though different combustion characteristics (e.g., temperature and gas concentration) were predicted reasonably well by all models [44].

Farokhi et al. [17] conducted a computational study on a small-scale biomass furnace. They investigated the effect of STD, RNG, and RKE $k-\varepsilon$ models against SFM and EDC models. After comparing the predictions with the experimental results, they found that although all three examined models produced similar predictions, RNG $k-\varepsilon$ model predicted local temperature region slightly better.

2.3.2 Radiation Models

Radiation is the dominant heat transfer process during solid fuel (i.e., biomass) combustion, and heat transfer has a significant impact on combustion occurring in a fixed bed furnace. Both combustion on the bed and freeboard space is affected directly by the radiative heat transfer rate as it controls the drying and devolatilization on the bed and heat distribution in the furnace. The chemical kinetics rate of the volatiles-air mixture in the freeboard space is critically dependent on heat distribution. Thus, radiative heat transfer affects different species concentrations resulting from the combustion. To account for radiative heat transfer, different radiation models are adopted in the modelling of combustion in a biomass furnace. Radiation models that are adopted in CFD modelling differ in their accuracy and computational cost. Radiation models can be divided into two groups. Group 1 includes the Discrete Ordinate model, the P1 model (Differential Approximation model), Rosseland Model, Discrete Transfer Radiation Model, and The Monte Carlo model, which solves for radiative direction [50]. Group 2 consists of Spectral models that include the Weighted Sum of Gray Gases Model, the Gray Model and the Multiband Model, and this group solves the radiation level of energy on the electromagnetic spectrum [51].

Very few investigations have been conducted on the numerical modelling of grate-firing biomass furnaces where the effect of different radiation models has been investigated. Klason et al. [36] compared four different radiation models: The optically thin (OT) model, P_1-approximation model, Finite volume discretization (FGG), and Weighted-sum-of-grey-gases model (SLW) for modelling combustion in two different biomass furnaces. They compared their predictions with the experimental results and concluded that the computational time of the P_1 model is lower compared to the other two models. They recommended utilizing the P_1-approximation model if the flame temperature in the furnace is the main concern. Another study was conducted by Ferreira et al.

[52], where they modelled the gas combustion in a sugarcane bagasse boiler. In this investigation, they adopted the P_1-approximation model and the Discrete transfer method (DTM) as the radiation models and reported similar results for both models.

2.3.3 Combustion Models

Gas-phase combustion model plays a crucial role in the prediction of temperature field and emissions. In general terms, a combustion model is responsible for the coupling between the chemical kinetics and flowfield [37]–[39]. Different combustion models have been introduced and applied in pursuit of providing a reliable CFD platform to conduct numerical investigations on the combustion of biomass furnaces. Combustion models can be divided into two main categories: species transport models (i.e., EDM, FRK/EDM and EDC) and mixture fraction-based models (i.e., non-premixed, partially premixed and premixed models) [41]. Species transport models require the individual calculation of conservation equations for describing diffusion, convection and reaction sources for each species for modelling the mixing and transport of the involved chemical species; whereas mixture fraction-based models do not require individual calculation, as it is estimated from the predicted mixture fraction field [41]. This is the contributing factor behind the high computational cost of the species transport models over the mixture fraction-based models.

Species transport models: Eddy dissipation concept (EDC) is the most commonly used combustion model for simulating gas-phase combustion in biomass furnaces when using reduced or detailed chemical reaction mechanisms. This model was proposed by Magnussen [29] in order to overcome the inability of the finite-rate kinetic/eddy dissipation model (FRK/EDM) to account for detailed chemistry under mixing limited conditions [31]. The applicability of EDC has been tested for various biomass combustion systems [9], [13], [53]–

[55]. Adequate predictions of premixed, partially premixed and non-premixed combustion regimes were achieved when using the EDC model (e.g., [56]). EDC model was originally developed for high turbulent flow conditions, while gas combustion inside a biomass grate furnace consists of both highly (e.g., at the inlet of secondary and tertiary air) and weakly (e.g., in the vicinity of the bed) turbulent flow regimes [31]. A sensitivity analysis on EDC (i.e., standard EDC) coefficients for weakly and highly turbulent conditions was conducted by Farokhi and Birouk [31], and their study showed that the model's predictions could be significantly improved at both weakly and highly turbulent flow conditions if the coefficients of the model are to be modified on the basis of turbulent flow characteristics (e.g., turbulent Reynolds number and time scale). However, this makes its use for simulating complex industrial geometries, where the reacting flow might occur under a variety of turbulent conditions, challenging if the model's coefficients are selected based on a particular turbulent reacting flow condition [31]. Some attempts to improve the applicability of EDC over a wide range of flow conditions have been proposed but focused on addressing predominantly premixed conditions in the MILD (Moderate or Intense Low-oxygen Dilution) combustion regime [55], [57]–[61]. A detailed review of these models can be found elsewhere [62]. To overcome this limitation, Farokhi and Birouk [63] proposed a modified EDC model, also known as the extended EDC model, to simulate a reacting flow field under different turbulent conditions, which reflects the real situation in an industrial biomass furnace. This new extended EDC model produced better results than the standard EDC version ([16], [63]). However, the high computational cost of both standard EDC and extended EDC, especially caused by detailed chemistry, made it difficult to simulate industrial (large) combustion plants [64]. In an attempt to reduce the computational time while still using a detailed chemical scheme, Farokhi

and Birouk [65] proposed a hybrid EDC/Flamelet model, where a pre-calculated flamelet was coupled with the extended EDC, and thus a lower computational time with a detailed chemical scheme could be achieved. While this model was able to predict reasonably well the temperature and major species, it was only capable of adequately predicting the trend of the slow-forming species (i.e., CO).

Mixture fraction-based models: Combustion models can still adopt detailed chemistry without increasing the computational cost when using mixture fraction-based models (e.g., steady/unsteady flamelet model (SFM/UFM) [66], [67]). However, these mixture fraction-based models have been used only in a few studies related to biomass combustion (e.g., [13], [17], [32]). The usage of SFM/UFM is limited to small/lab-scale biomass combustors because, given the complex and large geometry of industrial grate-firing biomass furnaces, the volatile gases released from solid biomass fuels cannot be expressed using only one single variable (i.e., mixture fraction) [68]. The applicability of the SFM approach to model a small furnace using packed-bed wood as fuel was investigated by Borello et al. [69] to predict ash formation and trajectories and evaluate the combustion completion rate based on the exhaust gas compositions. Although the SFM model is suitable for fast chemistry assumption [41], it showed a poor prediction of slow-forming species like CO and NO_x when simulating different turbulent flame regimes (i.e., premixed and non-premixed) [70]–[72]. This handicap was resolved using an unsteady flamelet model (UFM) that is capable of considering the transient history of the strain rate [41]. Farokhi et al. [17] conducted a computational study on a small grate-firing biomass furnace to investigate the gas-phase combustion using both SFM and UFM models with detailed chemical kinetic mechanisms and compared the results with published experimental measurements. They showed that the UFM model is capable of

resolving the handicap faced by the SFM model in predicting slow-forming species (e.g., CO). Their results indicate that although the mixture fraction-based models (i.e., SFM and UFM) seem to be a viable replacement for EDC-based models, SFM and UFM models are incapable of properly simulating combustion regime inside a biomass furnace because these models are purely non-premixed model.

The gas-phase mixing above the fuel bed of a grate-firing biomass furnace is greatly influenced by the character of the flow field (mainly weakly to moderately turbulent flow conditions close to the fuel bed and highly turbulent flow conditions close to secondary/tertiary air inlet injectors within the freeboard) [16], [33]. Referring to the various degrees of local mixing between the oxidizer and fuel, Shiehnejadhesar et al. [33]–[35] have termed the gas phase combustion in a grate-firing biomass furnace as partially premixed combustion. This may involve the coexistence of premixed and non-premixed combustion regimes inside a biomass furnace which cannot be simulated properly using a non-premixed model like SFM or UFM.

The coexistence of different turbulent flame regimes (i.e., premixed and non-premixed) within a large reaction zone (e.g., MILD combustors) has been reported in the literature (e.g., [63], [73]). In order to address the coexistence of turbulent flame regimes within a large combustion scale using a single combustion model, a fractal wrinkling/eddy dissipation-based combustion model has been proposed by Farokhi and Birouk [74]. But this attempt has been limited to a MILD combustor. No further investigation has been conducted to determine if this coexistence phenomenon of different combustion regimes inside a biomass furnace has an influence on the predictions of different combustion models.

2.4 Summary

Based on the literature discussed above, it is clear that there is a need for further research to develop a better combustion modelling strategy to deal with the coexistence of different combustion regimes (i.e., premixed and non-premixed combustion regimes) inside a biomass furnace. This coexistence phenomenon has been induced by the partially premixed nature of the volatile gases coming out of the bed in a grate-firing biomass furnace. Literature shows that species transport models' inability to incorporate detailed chemical mechanisms without compromising the computational cost has pushed researchers to explore the viability of other alternative combustion models for modelling the gas-phase combustion of biomass furnaces, such as mixture fraction-based models (i.e., flamelet-based models) [32]. Despite the fact that partially premixed models (i.e., flamelet-based model) have the ability to combine both premixed and non-premixed models [75], they have not been tested for modelling the gas phase of biomass combustion, as witnessed by the aforementioned literature. Thus, the present numerical investigation addresses this gap by exploring the capability of partially premixed combustion models for the simulation of the gas-phase combustion of a biomass furnace.

Chapter 3 METHODOLOGY

3.1 Overview of Numerical Model

Gas-phase combustion in the freeboard section is simulated, assuming a low Mach number gas flow approximation that obeys the ideal gas law. Reynolds Averaged Navier-Stokes (RANS) equations of momentum, continuity, energy and species transport are solved. Moreover, species diffusion in the energy equation due to enthalpy transport is also considered in this study. Additionally, a detailed chemical kinetic reaction mechanism has been adopted, which has previously been developed to define the combustion of volatile gases originating from the bed during the conversion process of biomass [76], [77]. To describe the flow field in the vicinity of the walls, an enhanced wall treatment approach [78] has been adopted, which utilizes an enhanced wall function (e.g., the suggested blending function by Kader [79]) for combining a two-layer approach (i.e., linear for the laminar region, and logarithmic for the turbulent region) [30], [41]. Ref. [41] presents a detailed explanation of this model. The P-1 approximation model and RNG (i.e., Renormalizing Group) $k-\varepsilon$ model have been adopted as the radiation and the turbulence model, respectively. Their selection were done on the basis of previous studies mentioned in Chapter 2. Previously conducted research on the same geometry as in the current study shows that the selected models performed better with reasonable accuracy compared to other alternate counterparts. The simple particle-based bed model adopted in this study. Partially premixed combustion models are applied and evaluated in the present study based on the research gaps as mentioned in Chapter 2. Moreover, the prediction ability of these models will also compared against other combustion models (i.e., SFM, UFM and EDC-Flamelet model). A detailed description of the selected sub-models is given below.

3.1.1 Radiation Model

In order to address the heat transfer by radiation, the P-1 approximation model [80] is adopted with the domain-based weighted-sum-of-gray-gas (WSGG) method [81]. The selection of the P-1 radiation model was based on the outcome of previous studies on the same furnace with the same operating condition, where a comprehensive sensitivity analysis on the effect of the chosen radiation model on the predictions. The latter revealed that the P-1 approximation model along with the WSGG method resulted in acceptable performance at low computational cost [36].

In order to address the local incident radiation present in the computational domain, the following equation is solved in the P_1 radiation model [6], [41]:

$$\nabla.\left(\frac{1}{3(a+\sigma_s)-C\sigma_s}\nabla G\right)-aG+4an^2\sigma T^4=0 \quad (1)$$

Where C, a and σ_s denote a linear-anisotropic phase function coefficient, the absorption and the scattering coefficients, respectively. The refractive index of the medium and the Stefan-Boltzmann constant is denoted by n and σ [6], [41]. The radiation heat flux's effect has been introduced as a source term in the following equation (i.e., S_h) [41] as the radiation heat flux has been defined as $q_r=-\nabla G/(3(a+\sigma_s)-C\sigma_s)$ [6], [41]:

$$S_h=-\nabla.q_r=aG-4an^2\sigma T^4 \quad (2)$$

The absorption coefficient (a) in Eq. (1) has been addressed by adopting the Weighted-sum-of-Gray-Gases (WSGG) approach, and the total emissivity over a distance of 's' is approximated in the WSGG model solving the following equation:

$$\varepsilon=\sum_{i=0}^{I}a_{\varepsilon,i}(T)(1-e^{-k_iPs}) \quad (3)$$

Where $a_{\varepsilon,i}(T)$, k_i and P denotes the emissivity weighting factor of the ith fictitious gray gas as a function of temperature, the absorption coefficient of the ith gray gas and the sum of the partial pressures of all absorbing gases, respectively. The derived values of $a_{\varepsilon,i}$ and k_i from the works by Coppalle and Vervisch [82] and Smith et al. [83] have been documented in FLUENT's database. Eq. (3) can be simplified as $\varepsilon = \sum_{i=0}^{I} a_{\varepsilon,i} k_i P s$ if the value of $k_i P s$ is much smaller than unity for all absorbing gases and the following equation can be used for the approximation of absorption coefficient (a) adopting this estimated value of the emissivity (ε) [41]:

$$a = \sum_{i=0}^{I} a_{\varepsilon,i} k_i P \quad s < 10^{-4}[m] \tag{4}$$

$$a = \frac{-\ln(1-\varepsilon)}{s} \quad s > 10^{-4}[m] \tag{5}$$

3.1.2 Turbulence Model

RNG (i.e., Renormalizing Group) $k-\varepsilon$ turbulence model [46] is selected for accounting for the turbulence of the flowfield. It has been reported to be the most optimum turbulence model in a previously conducted sensitivity analysis on the current furnace using similar operating conditions [17]. Unlike large eddy simulation and Reynolds-Stress Model (RSM), RANS framework, two-equation-based RANS models such as RNG $k-\varepsilon$ model are well-known for their lack of appropriate predictions of turbulent length/time scales due to their simplified assumption of Reynolds Stress modeling [41]. However, it is important to mention that the two-equation RANS models are still one of the most popular turbulence models for modelling large domains of industrial CFD applications due mainly to their robustness, simplicity and computational cost [41]. Renormalization group theory, which is a statistical technique, has been utilized for the derivation of the RNG $k-\varepsilon$ model. Similar form of transport equations are solved by both STD and RNG $k-\varepsilon$

model for calculating turbulent kinetic energy, k and its rate of dissipation, ε. The ε equation solved in the case of RNG model includes an additional term that enhances accuracy when modelling flows that are rapidly strained. The transport equations of this model are given as follows [41]:

$$\frac{\partial}{\partial t}(\rho k) + \frac{\partial}{\partial x_i}(\rho k u_i) = \frac{\partial}{\partial x_j}\left(a_k \mu_{eff} \frac{\partial k}{\partial x_j}\right) + G_k + G_b - \rho\varepsilon - Y_M + S_k \quad (6)$$

$$\frac{\partial}{\partial t}(\rho \varepsilon) + \frac{\partial}{\partial x_i}(\rho \varepsilon u_i) = \frac{\partial}{\partial x_j}\left(a_\varepsilon \mu_{eff} \frac{\partial \varepsilon}{\partial x_j}\right) + C_1 \frac{\varepsilon}{k}(G_k + C_{3\varepsilon} G_b) - C_2 \rho \frac{\varepsilon^2}{k} - R_\varepsilon + S_\varepsilon \quad (7)$$

where, G_k and G_b denote turbulence kinetic energy generation caused by the mean velocity gradient and buoyancy, respectively. Y_M denotes fluctuating dilatation contribution in compressible turbulence to the overall dissipation rate, and a_k and a_ε denote, respectively, the inverse Prandtl number for k and ε. S_k and S_ε denote the source terms [41].

3.1.3 Bed Model

For this study, a simplified particle-based bed model has been adopted, and a discrete phase model (DPM) has been employed in order to execute the solid fuel conversion process in ANSYS Fluent [41]. Different sub-models are being offered by the standard DPM model in Fluent to describe char combustion and thermal conversion, which enhances its capability to model the bed section satisfactorily [84]. In spite of this capability, this methodology can not handle particle tracking in a fixed condition because of its inability to consider particle-particle collisions [84]. In this methodology, the particles are considered to be equivalent to a spherical particle having a uniform temperature all around its body [85]. Both radiation and convection methods are considered to account for heat transfer; however, the convection method is limited to particle-gas interaction. Vaporization and boiling are the two sub-processes that are considered to tackle the drying process

in the bed section [17]. The embedded vaporization law in DPM considers that liquid water in the particles maintains a thermodynamic equilibrium condition with the local vaporized water [41], [86]. Furthermore, a diffusion-controlled vaporization rate is considered [84], [86]. The adopted convection/diffusion-controlled vaporization rate for this current study can be expressed as follows [41], [87]:

$$\frac{dm_p}{dt} = \rho K_c A_p \ln\left(1 + \frac{Y_{w,s} - Y_w}{1 - Y_{w,s}}\right) \tag{8}$$

where m_p, A_p, ρ, $Y_{w,s}$ and Y_w denote the particle's mass and surface area, the bulk gas density, the mass fractions of vapour at the surface and the mass fractions of vapour in the bulk gas, respectively. Convection and radiation heat transfer methods are implied for determining the particle temperature as follows [41]:

$$m_p C_p \frac{dT_p}{dt} = hA_p\left(T - T_p\right) - \frac{dm_p}{dt} h_{fg} + A_p \varepsilon \sigma (\theta^4 - T_p^4) \tag{9}$$

where T, C_p, h_{fg}, ε, σ and $\theta = (0.25G/\sigma)^{0.25}$ denote the bulk gas temperature, the latent heat of water, the particle's emissivity, the Stefan-Boltzmann constant and radiation temperature (G is the incident radiation [41]). From Sherwood and Nusselt number correlations, the diffusion mass transfer coefficient (K_c) and convective heat transfer coefficient (h) are calculated, respectively, as follows [41], [88], [89]:

$$K_c = \frac{D_{w,m}\left(2 + 0.6 Re_d^{1/2} Sc^{1/3}\right)}{d_p} \tag{10}$$

$$\frac{h d_p}{k} = \frac{Y_{w,s} - Y_w}{1 - Y_{w,s}}\left(2 + 0.6 Re_d^{1/2} Pr^{1/3}\right) \tag{11}$$

where the diffusion coefficient of vapour in bulk gas, the particle's diameter, the thermal conductivity of the bulk gas, the particle's Reynolds number [41], Schmidt and Prandtl number of the bulk gas are denoted by $D_{w,m}$, d_p, k, Re_d, Sc and Pr, respectively.

The transition between the vaporization and drying process is determined by the particle's temperature. The vaporization process prolongs throughout the time while the particle's temperature remains between the vaporization temperature (i.e., T_{vap}= 284 K) and boiling temperature (i.e., T_{boil}= 373 K) and switches to the drying process as soon as the temperature of the particle attains T_{boil}. Heat transfer rate controls the drying rate and is determined by the following equation [84]:

$$h_{fg}\frac{dm_p}{dt} = hA_p\left(T - T_p\right) + A_p\varepsilon\sigma(\theta^4 - T_p^4) \quad (12)$$

In order to account for the devolatilization process, a simplified devolatilization model is adopted that uses a single-step kinetic rate for calculating the devolatilization rate and the mass exchange rate during this process can be expressed by the following equation [84]:

$$\frac{dm_p}{dt} = -A\exp\left(-\frac{E}{RT}\right)\left[m_p - (1 - Y_{v,0})(1 - Y_{w,0})m_{p,0}\right] \quad (13)$$

where the initial mass of the particle, the initial mass fractions of moisture in the particle, the initial volatile in the particle and the universal gas constant are denoted by $m_{p,0}$, $Y_{w,0}$, $Y_{v,0}$ and R, respectively, and the conversion rate constants are A = 1.5e-2 s^{-1} and E=20 kJ/mol [90]. CO, CO_2, H_2O, H_2, NH_3 and CH_4 as light gas/hydrocarbons [86], and levoglucosan ($C_6H_{10}O_5$) as a representative of heavy hydrocarbon have been assumed to be the emitted volatile gases due to the devolatilization process.

The assumption of mass fractions of released species in the devolatilization process is used following the work of Thunman et al. [91]. A single chemical composition along with char can be accommodated in the DPM approach, and so the first step consists of an artificial species where all the light and heavy hydrocarbons are lumped together, and this artificial species carries an equivalent amount of mass and energy of the mixture of volatile gases. The ultimate and proximate analysis of the used biomass fuel particles is then used to determine the composition of the artificial hydrocarbons. The mass fraction of each species is determined for each iteration in the bed section by employing a UDF code that is documented in Ref. [16].

During the depletion of oxygen, the gasification of char is considered to be of great importance as the char oxidation procedure is remarkably quicker than the gasification procedure of char [91]. Due to the nature of the adopted furnace (i.e., updraft fuel feeding system), the volatile gases are more prone to be released from a position on the bed which is prior to the position where char formation may initiate. This phenomenon is also caused by the limitation of the DPM approach that initiates heterogeneous reactions after the complete conversion of fuel particles into volatile gases [41], which leads to considering char oxidation with primary air. CO_2 and CO are the primary products of char oxidation, and the oxidation state (partially or fully) of char impacts the CO/CO_2 ratio [86]. Nevertheless, in the present study, CO has been presumed to be the only char product for simplification and this assumption is supported by previous literature (e.g., [48], [84], [92]) since the main char oxidation product of woody particles is CO [84]. A combination of oxygen diffusion rate and the chemical kinetic rate has been adopted to determine the char combustion rate using the following equation [86]:

$$\frac{dm_p}{dt} = -A_p \left(\frac{\rho R T Y_{ox}}{MW_{ox}}\right) \frac{R_{dif} R_{kin}}{R_{dif} + R_{kin}} \quad (14)$$

where Y_{ox}, MW_{ox}, R_{kin} and R_{dif} denote the mass fraction of the oxidizer, the molecular weight of the oxidizer, the kinetic rates of char combustion, and diffusion rates of char combustion. A detailed description of char oxidation and its kinetic and diffusion rates are well documented in Refs. [19], [93], [94]. Details of the adopted fuel properties can be found in Refs. [6], [95] and are presented in Table 1.

Table 1. Fuel properties [95]

Ultimate analysis dry ash-free basis (wt%)				**Proximate analysis (wt%)**			
C	**O**	**H**	**N**	**Volatile**	**Fixed Carbon**	**Moisture**	**Ash**
51.1	42.5	6.3	<0.1	79.4	14.2	6.0	0.4

In addition to the adoption of a simple particle-based bed model, the average mass fraction of different species coming out of the fuel bed was also calculated following the work of Patronelli et al. [96]. In their study, the entire bed was assumed to be a perfectly stirred reactor, and under this assumption, the following order of thermal conversion processes occur depending on the surface reaction mechanism and volatile compositions considered in the bed model.

$$Wet\ biomass \rightarrow Moisture + Dry\ biomass \quad (15)$$

$$Dry\ biomass \rightarrow Volatile(CO, CO_2, H_2O, CH_4, C_6H_{10}O_5, NH_3) + Char \quad (16)$$

$$Char + 0.5O_2 \rightarrow CO \quad (17)$$

The average mass fraction of the species was calculated considering the proximate and ultimate analysis of the biomass fuel documented in Table 1, along with the conservation of elemental mass (i.e., C, H, O and N).

3.1.4 Combustion Models

For this study, four different combustion models were tested (i.e., SFM, UFM, partially premixed and EDC/Flamelet) as reported in Table 2. In the case of SFM, rather than solving individual transport equations for each gas-phase species, it only calculates the mean enthalpy, mean mixture fraction and means mixture fraction variance [17]. A flamelet library is generated and tabulated from one-dimensional (1D) laminar flamelet structures, which addresses the effects of detailed chemistry [13], [97]. By transferring data (i.e., species mass fraction and temperature) from the flamelet (physical space) into the mixture fraction space, the generated flamelet is embedded in the turbulent reacting flow. This allows describing the temperature and species mass fraction as functions of the local mixture fraction and local scalar dissipation rate [13], [41], [97]. A probability density function (PDF) of mixture fraction, scalar dissipation rate and enthalpy are adopted to address the influence of diffusion flamelet into a turbulent reacting flow [17]. The commercial software ANSYS Fluent also uses the ‘Automatic Grid Refinement (AGR)’ method for improving the prediction accuracy in the local high gradient of flow and combustion characteristics [41].

Table 2. Combustion models

Partially Premixed Model (with different combinations)						
Case	**Radiation Model**	**Premixed Model**	**State Relation**	**Kinetic Reaction Mechanism**	**Turbulence Model**	**Boundary Conditions**
Case 1	P1	Extended Coherent Flame Model	Steady Diffusion Flamelet (SFM)	Detailed	RNG	BC-1
Case 2	P1	C Equation			RNG	
Case 3	P1	C Equation	Unsteady Diffusion Flamelet (UFM)		RNG	
Case 4	P1	C Equation			RNG	BC-2
Case 4b	P1	C Equation	Steady Diffusion Flamelet (SFM)		RNG	
Other combustion models						
Case	**Combustion Model**	**Radiation Model**		**Kinetic Reaction Mechanism**	**Turbulence Model**	**Boundary Conditions**
Case 5	EDC-Flamelet	P1		Detailed	RNG	BC-2
Case 6	SFM	P1			RNG	BC-1
Case 7	UFM	P1			RNG	BC-1

The process of coupling turbulent flow field and chemistry in a flamelet approach is accomplished through the flow field strain rate, which is correlated to a term known as scalar dissipation rate [71]. The prediction inaccuracy of slow chemistry species by SFM results from assuming a steady-state solution for all species despite steep changes in the strain rate [98]. Unlike SFM, UFM takes the effect of unsteadiness of strain rate into consideration and is capable of producing improved prediction of slow-forming species [17]. In order to address the unsteadiness effect, UFM performs post-processing of the converged flow field of SFM and utilizes the transient history of the scalar dissipation rate evolution [41], [71]. Any significant influence due to the transient effect could only be observed in the case of only slow-forming species [17], [67]. Consequently, it is expected that UFM will be most influential on slow chemistry species as opposed to SFM.

A partially premixed combustion model has also been adopted, and its predictions will be compared with the results of previous studies [65]. The partially premixed model combines both non-premixed and premixed combustion models [41], so its capability to address the coexistence of premixed and non-premixed turbulent flame regions in the reaction zone of a grate furnace has been examined in this study. Two mixture fraction-based partially premixed models have been examined in this study, known as reaction progress variable based (i.e., C equation) and extended coherent based partially premixed model. In the steady diffusion flamelet partially premixed model, the premixed flame front is assumed to be infinitely thin [41]. Under this assumption of a thin flame front, for the reaction progress variable-based model, density-weighted mean scalars (i.e., temperature and species fractions, $\overline{\emptyset}$) are calculated using the following equation:

$$\overline{\emptyset} = \bar{c} \int_0^1 \emptyset_b(f)p(f)df + (1-\bar{c}) \int_0^1 \emptyset_u(f)p(f)df \quad (18)$$

where $p(f)$ and $\bar{c}$ represent the probability density function (PDF) of *f*, and the mean reaction progress variable, respectively [41]. Here, burnt products and unburnt reactants are denoted by subscripts *b* and *u*, respectively. The burnt scalar, $\emptyset_b$ is the function of the mixture fraction, and it can be calculated by mixing a mass f of fuel with a mass $(1-f)$ of oxidizer and allowing the mixture to achieve equilibrium, where *f* represents the mixture fraction. Similarly, the unburnt scalar, $\emptyset_u$ is calculated by mixing a mass f of fuel with a mass $(1-f)$ of oxidizer, where the mixture is not combusted. When using the C equation-based partially premixed model, the value of the mean reaction progress variable (i.e., C) is derived using a transport equation of $\bar{c}$ which describes the spatial and temporal evolution of the reaction progress in the flow field as follows [41]:

$$\frac{\partial}{\partial t}(\rho\bar{c}) + \nabla.(\rho\vec{u}\bar{c}) = \nabla.\left(\frac{\mu_t}{Sc_t}\nabla\bar{c}\right) + \rho S_c \quad (19)$$

where Sc_t, μ_t, ρ and S_c denote, respectively, turbulent Schmidt number, turbulent viscosity, density and reaction progress source term, which is expressed as $\rho S_c = \rho_u U_t|\nabla c|$ (ρ_u and U_t represent unburnt mixture density and turbulent flame speed, respectively).

Compared to the C equation model, the extended coherent flamelet model (ECFM) is considered to be more refined because of its greater theoretical accuracy [41]. An additional equation is solved by the ECFM model for the flame area density, which is used later on as a new reaction progress source term to model the reaction progress variable in Eq. (19). The increased flame surface area in this model is caused by the assumption that laminar flame thickness is smaller than the smallest turbulence length scales (e.g., Kolmogorov eddies) [41]. Increased net fuel consumption and flame speed can be attributed to this increment in flame surface area. The additional solved equation to calculate the flame area density is:

$$\frac{\partial \Sigma}{\partial t} + \nabla.(\vec{u}\,\Sigma) = \nabla.\left(\frac{\mu_t}{Sc_t}\nabla\left(\frac{\Sigma}{\rho}\right)\right) + (P_1 + P_2 + P_3)\,\Sigma + P_4 - D \quad (20)$$

Where Σ and D denote the mean flame area density and dissipation of flame area (i.e., $D = 0.4U_l\frac{\Sigma^2}{1-\bar{C}}$ where U_l is the laminar flame speed), respectively [41]. The terms P_1=$1.6K_t$ (K_t as turbulent time scale [99]), $P_2 = \frac{2}{3}\rho\nabla(\rho\vec{u})$, $P_3 = 0.2\frac{U_l}{\bar{C}}\frac{\Sigma}{1-\bar{C}}$ and $P_4 = U_l\nabla^2\bar{C}$ denote source terms due to turbulence interactions, dilatation in the flame, expansion of burned gas, and normal propagation, respectively. Note that the mathematical expressions of P_1, P_2, P_3 and P_4 can be found in [99] and [41]. Finally, a new reaction progress source term (i.e., the last term on the right side of Eq. (19)) is introduced as $\rho S_c = \rho_u U_l \Sigma$ where U_l is the laminar flame speed [41].

The chemical calculations and PDF integrations for the burnt mixture are executed along with the construction of a look-up table in ANSYS Fluent, similar to the non-premixed steady flamelet model (SFM) and unsteady flamelet model (UFM). Settings utilized for the generation of the flamelet and PDF look-up table are reported in Table 3. In addition, another simulation was conducted with different settings (Grid point: 60 & Scalar dissipation step: 0.5), and the derived results revealed an almost identical outcome.

Table 3. Settings for the generation of flamelet and PDF look-up table

Parameter	**Value [unit]**
Maximum number of flamelets	20 [-]
Number of flamelet grid points	32 [-]
Number of scalar dissipation step	2.5 [-]
Initial scalar dissipation	0.005 [S^{-1}]
Scalar Dissipation Multiplier	5 [-]
Number of mean mixture fraction points in PDF table	50 [-]
Number of fraction variance point in PDF table	30 [-]
Number of mean enthalpy points in PDF table	30 [-]
Maximum number of species	137 [-]
Minimum temperature	298 [K]

EDC/Flamelet hybrid model was proposed by Farokhi and Birouk [65], and it was developed on the platform of an extended version of EDC [63]. Incorporating a detailed chemical mechanism in EDC comes with an extensive computational cost, and therefore EDC/Flamelet model was introduced to overcome this handicap. Unlike previous studies [56], [100] where a tabulated chemical time-scale (obtained by detailed chemistry) along with the assumption of fast chemistry was used in determining the chemical reaction rate, a pre-calculated steady laminar flamelet database was adopted in this model to account for detailed chemistry. Additionally, the mass fraction of species was also extracted from the adopted flamelet database within fine structures rather than resolving real-time chemical kinetics rates [65]. A more detailed description can be found elsewhere [65].

Chapter 4 PHYSICAL AND NUMERICAL SETUP

A schematic view of the physical setup is illustrated in Figure 2. Details about the lab-scale biomass furnace are provided in [6], [95], so only a brief description is given below. The small lab-scale furnace has a power capacity of 8-11 kW and consists of a cylindrical combustor with a 0.2 m diameter. The primary air enters the furnace from underneath the grate, situated at the bottom of the bed, at a mass flow rate of 0.581e-3 kg/s. More air enters the furnace through the secondary and tertiary air inlets located above the bed at a mass flow rate of 1.18e-3 kg/s and 1.89e-3 kg/s, respectively. Pressure and temperature of all airflows at the inlet are maintained constant at 100 Kpa, and 298 K. Wood pellets (diameter- 0.006 m and length – 0.0065 m) are fed into the furnace bed at a mass flow rate of 0.461e-3 kg/s. The feed rate was controlled within ± 2% of the mean mass flow rate with a few occasional fluctuations due to difficulties in controlling the mass flow rate, which could be the cause of emission fluctuations at the outlet [95]. The measured temperatures of the volatile gases close to the bed and the furnace's wall are, respectively, 1373.15 K and 873.15 K. These two values have been adopted for the inlet temperature of volatile gases and wall temperature.

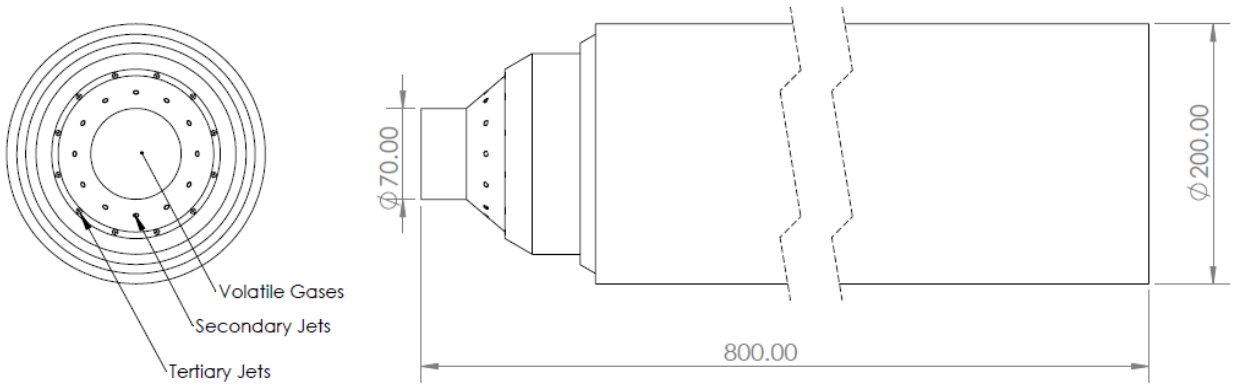

Figure 2. Schematic diagram of an 8-11 kW grate firing biomass furnace [6].

ANSYS-FLUENT 19.2 has been used for performing the CFD simulations. All conservation equations described above were solved by adopting the second-order upwind spatial discretization scheme using the velocity-pressure coupling method. A 3D non-uniform/unstructured grid consisting of 508619 cells has been used for modelling the furnace geometry that covers 820 mm above the bed. A local increase in grid resolution has been applied in the vicinity of the bed and at the secondary and tertiary jet exit locations. The axial temperature and velocity were compared for four cases of grid number (i.e., coarse-1 with 240888 elements, coarse-2 with 393583 elements, fine-1 with 508609 elements and fine-2 with 549409 elements), and the results showed no significant change in the species concentration predictions as well as velocity and temperature profile along the centerline with further grid refinement beyond grid fine-1, and hence, fine-1 grid was selected for this study. Detailed mesh independency analysis has been documented in APPENDIX A.

For defining wall conditions, zero normal gradients of species accompanied by non-slip conditions and a constant temperature of 873.15 K have been adopted, and the bed and wall emissivity has been set as 0.9 [6], [36]. An outflow boundary has been defined as a pressure outlet. All adopted boundary conditions have been documented in Table 4. The choice of numerical settings is based on previously published studies on the same furnace with a similar grid and numerical framework (e.g., [17], [20], [36], [101]) and also in accordance with ANSYS Fluent guidelines in the best practice of numerical setup. The choice of boundary conditions and numerical framework (e.g., radiation model, turbulence model, etc.) also have been based on published studies on the same furnace (e.g., [17], [20], [36], [101]).

Table 4. Inlet boundary conditions [6]

Boundary Conditions		**BC-1**			**BC-2**		
Inlet		**Primary**	**Secondary**	**Tertiary**	**Primary**	**Secondary**	**Tertiary**
Species (Mass Fraction)	$C_6H_{10}O_5$	0.0686	-	-	0.005411	-	-
	CH_4	0.0686	-	-	0.067688	-	-
	CO_2	0.0428	-	-	0.074089	-	-
	O_2	0.046	0.233	0.233	0.042418	0.233	0.233
	H_2O	0.07	-	-	0.122384	-	-
	CO	0.276	-	-	0.19302	-	-
	N_2	0.428	0.767	0.767	0.477945	0.767	0.767
	H_2	-	-	-	0.016467	-	-
	NH_3	5.04e-4	-	-	4.83e-4	-	-
Mass flow rate (m)	[kg/s]	1.04e-3	1.18e-3	1.89e-3	1.04e-3	1.18e-3	1.89e-3
Temperature (T)	[K]	1373	298	298	1050	298	298
Turbulence	I (%)	5	23	58	5	23	58
	L [m]	7e-2	4e-2	4e-2	7e-2	4e-2	4e-2

For this study, two different sets of bed boundary conditions have been tested, which are reported in Table 4. The two boundary conditions are referred to as BC-1 and BC-2 and are calculated from published studies, where a simple particle-based bed model was adopted to incorporate the conversion of a solid biomass fuel into an equivalent gas species (see [65] and [101]). BC-1 was calculated using equations (15),(16) and (17), assuming the entire bed as a perfectly stirred reactor (PSR) following the conservation of mass and energy between the fuel and air inlet against the gases coming out of the bed. The composition of gases coming out of the bed is assumed to consist of light volatile gases (i.e., CO, CO_2, H_2O, CH_4, O_2 and NH_3) along with $C_6H_{10}O_5$ as a representative of heavy hydrocarbon. In addition, the product of the surface reaction of char and O_2 is assumed to consist of CO that is already considered in the mass fraction of the total gases coming out of the bed. Details about the bed model and its results of species mass fractions for the same furnace with the same operating conditions can be found elsewhere [65]. The mass fractions of the aforementioned species calculated in [65] from the bed-stirred reactor were used as the inlet

conditions of the flamelet for representing the mixture fraction coming out of the bed. In the case of BC-2, in order to compare the partially premixed model against the EDC/Flamelet model, the predicted results of species mass fraction coming out of the bed are adopted from Ref. [65] for creating a pre-calculated flamelet library. In Ref. [65], porous zone CFD modelling approach was adopted considering an extended length (20.00 mm) of the furnace, which represents the length of the bed (not shown in Figure 2). Modelling of both, the bed section and the freeboard section, was coupled together in this study, and the simulation adopting the EDC/Flamelet model was initiated from the introduction of the biomass fuel into the bed, which caused the boundary condition prediction (i.e., BC-2) to differ from the former one (i.e., BC-1). Additionally, the assumption of light volatile gases by the two bed models also contributed to this difference. The presence of residual H_2 gas in BC-2 is due to the incomplete oxidation of H_2 gas in the bed which resulted in a lower inlet temperature of volatile gases compared to BC-1. On the other hand, BC-1 was calculated considering the completion of the devolatilization of the biomass fuel in the bed which assumes complete combustion of H_2 gas, which in turn caused a higher inlet temperature of the volatile gases at the inlet to the freeboard (Table 4). Table 1 shows the adopted fuel properties used for the calculation of the inlet boundary conditions. Table 4 illustrates the boundary conditions used to represent all inlet boundaries of the furnace for CFD simulation. Table 5 reports the mass balance between the inlet (i.e., solid/biomass fuel along with the primary air) and the outlet of the assumed bed-stirred reactor (i.e., gases coming out of the bed).

Table 5. Elemental mass balance between inlet and outlet of the bed

Mass flux (kg/s)		**C**	**H**	**O**	**N**
Ultimate analysis (fuel+air)		3.77e-5	4.99e-6	5.66e-5	7.43e-5
Calculations	BC-1	-3.68e-5	-5.08e-6	-5.74e-5	-7.43e-5
	BC-2	-3.70e-5	-4.83e-6	-5.59e-5	-7.42e-5
Relative error (%)	BC-1	2.36	1.89	1.42	0.22
	BC-2	1.74	3.06	1.36	0.24

Chapter 5 RESULT AND DISCUSSION

Table 2 summarizes all simulated cases in the present study. In order to evaluate the effect of partially premixed combustion models on the predictions of temperature and species concentration of the simulated furnace, different simulations were conducted that consisted of two partially premixed models: extended coherent flamelet model (case 1) and C- equation-based premixed model (case 2), with both cases use SFM to account for non-premixed combustion state of the reacting flow. A third case (case 3) is performed, which uses C-equation and UFM to take into account the premixed and non-premixed parts of the combustion model, respectively. In order to evaluate the performance of partially premixed models versus mixture fraction-based non-premixed models, two additional cases were simulated (cases 6 and 7), where SFM and UFM purely non-premixed models were adopted. Also, a sensitivity analysis is conducted using two different bed boundary conditions (i.e., top of the bed boundary with the freeboard, which represents the volatile gases coming out off the bed into the freeboard), which are referred to here as BC-1 (case 3) and BC-2 (case 4). Finally, a comparison between the predictions of the partially premixed combustion model (i.e., case 4b using C-equation and SFM) and the hybrid EDC/Flamelet model (i.e., case 5 using extended EDC along with SFM flamelet library) is performed with BC-2 is adopted as the bed boundary condition in both cases. Since the hybrid EDC/Flamelet model was previously studied [65], its results of the volatile gases coming out at the top of the bed surface are used to represent BC-2 in the present analysis. In the aforementioned simulated cases, the predicted temperature and species concentrations were compared with their published experimental counterparts (captured along the centerline) of the simulated furnace. The experimental measurements published in Refs. [6], [95] have been used for validating the simulations.

5.1 Effect of flamelet-based models: Partially premixed versus purely non-premixed

In this section, two different premixed models (i.e., the extended coherent flame model and the C-equation model) are compared against two different non-premixed models. In addition, a comparison between the predictions of temperature field and species concentrations of the aforementioned mixture fraction-based partially premixed models (i.e., cases 1, 2 and 3) and the two-mixture fraction-based non-premixed combustion models (i.e., SFM in case 6 and UFM in case 7) is presented.

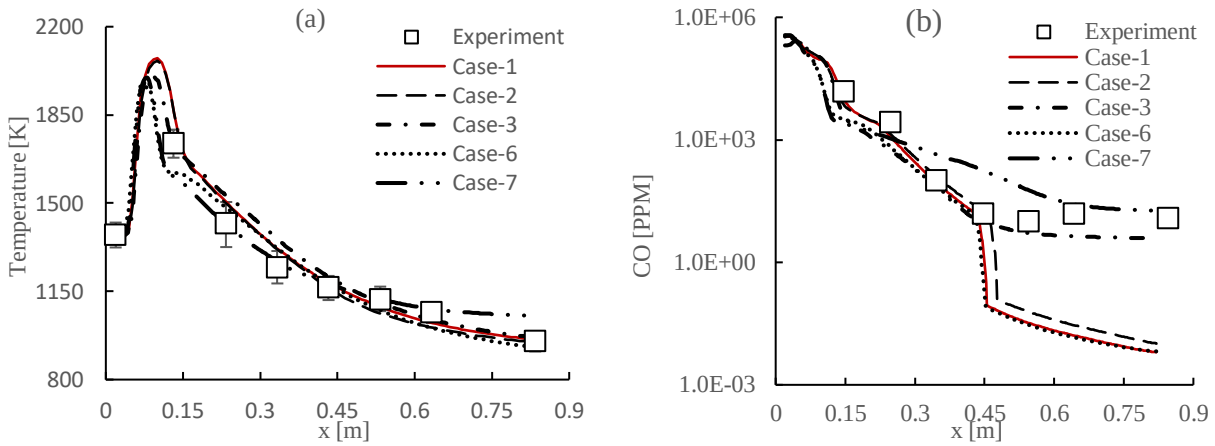

Figure 3. Comparison between numerical predictions and measurements of (a) Temperature and (b) *CO* concentration along the centreline of the furnace.

The predicted temperature profiles and the concentration of *CO* along the centerline of the furnace are presented in Figure 3(a) and (b), respectively. Figure 3(a) shows that, compared to measurements, all studied cases are able to satisfactorily predict the temperature profile along the centerline of the furnace. However, while the temperature prediction in cases 1, 2 and 3 is almost similar downstream of the furnace, both SFM and UFM that are purely non-premixed models (i.e., cases 6 & 7, respectively) show some differences in the temperature prediction in the local high-

temperature region (i.e., up to $x \approx 0.3\ m$). For instance, the peak temperature predicted by both non-premixed models (cases 6 and 7) is not only comparatively lower than those of cases 1, 2 and 3, but it is also established closer to the bed boundary. The predicted peak temperature in cases 1, 2, 3, 6 and 7 are 2075 K, 2065 K, 2004, 1993 K and 1998 K, respectively. In addition, UFM based non-premixed model (case 7) shows the lowest temperature up to $x \approx 0.3\ m$ and the highest after $x \approx 0.4\ m$. As for the other non-premixed model (case 6), while its prediction of the temperature is in agreement with the measurements beyond $x \approx 0.3\ m$, it produces overall similar results to case 7 for the bed region upstream of $x \approx 0.3\ m$. The discrepancy in the prediction of the local high-temperature region (i.e., up to $x \approx 0.3\ m$) between the partially premixed and purely non-premixed models will be explained later using species profiles of CH_2O and *OH* (Figure 5).

Figure 3(b) shows that the prediction of *CO* concentration by both partially premixed cases (cases 1 and 2) is quite similar, although a slightly higher concentration of *CO* is produced by C-equation (i.e., case-2) downstream of the furnace. Compared to the measurements, cases 1, 2 and 3 satisfactorily predict *CO* concentration up to the mid of the furnace ($x \approx 0.45\ m$). However, in the region of $x \sim > 0.45\ m$, cases 1 and 2 predictions drift significantly, as they underpredict *CO* concentration, whereas case 3 prediction is in closer agreement with the measurements. Figure 3(b) also shows that case 6 produces a similar prediction to cases 1 and 2 which they adopt SFM as a non-premixed model. On the contrary, when adopting UFM as the non-premixed model (case 7), *CO* species concentration is predicted to be slightly closer to that of case 3 but with a lesser agreement with the measurements, especially for the region between $x \approx 0.3\ m$, and $x \approx 0.6\ m$. These results clearly indicate that the prediction capability of the partially premixed combustion model of the slow-forming species (i.e., *CO*) is influenced by the adopted non-premixed combustion model, especially in the chemical equilibrium region of the furnace (i.e., downstream

of the local high-temperature region; $x\sim > 0.3\ m$). However, the results clearly show, that when adopting both UFM and C-equation in the partially premixed combustion model, the simulation predictions of *CO* species are in good agreement with the measurements. A scalar dissipation rate analysis has been conducted in order to determine the presence of a chemical equilibrium state, and the result has been documented in APPENDIX B.

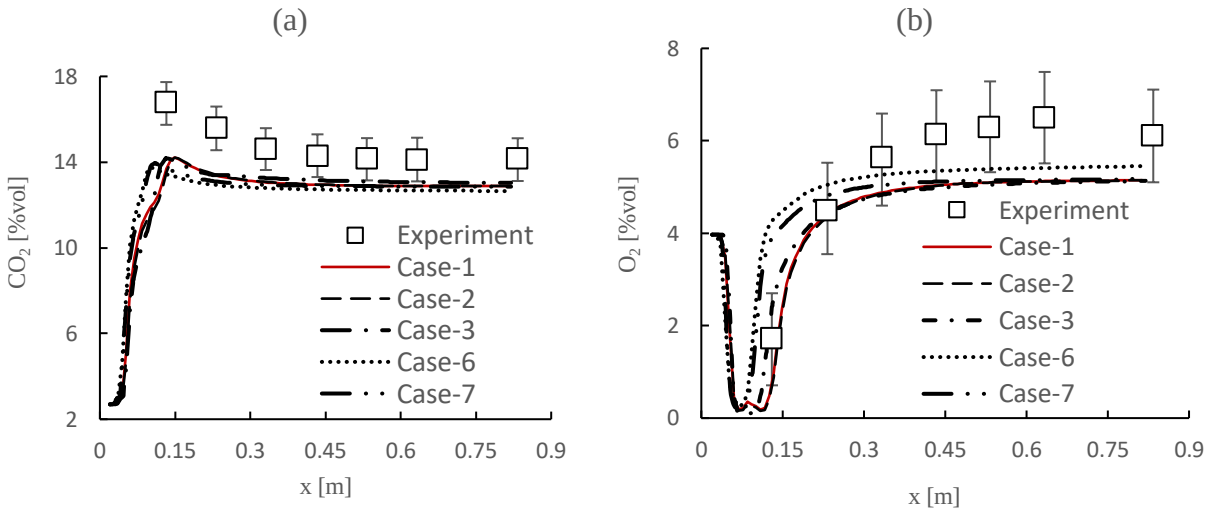

Figure 4. Comparison of the predictions with measurements of (a) CO_2 mole fraction and (b) O_2 mole fraction along the centerline of the furnace.

The predictions of CO_2 and O_2 mole fractions along the centerline of the furnace are shown in Figure 4(a) and (b), respectively. These figures show that, compared to the measurements, the prediction made by all cases reveals a similar trend/profile. The underprediction of CO_2 mole fraction in the local high-temperature region is likely due to the enhanced dissociation of CO_2 [102], which also yields the prediction of higher *CO* concentration in the same region. In addition, the overall lower quantitative prediction of both CO_2 and O_2 in all cases indicates that the mixture fraction-based models tend to underpredict the fuel consumption in the equilibrium region downstream of the furnace, whereas the hybrid EDC/flamelet model (see Figure 11) produces much better quantitative predictions when compared to the measurements and those of SFM and

UFM shown in Figure 4. Figure 4 clearly indicates that cases 1, 2 and 3 produce similar results, which imply that the partially premixed model is capable of predicting CO_2 and O_2 mole fraction satisfactorily throughout the furnace irrespective of the adopted premixed or non-premixed model. On the other hand, when used independently (cases 6 and 7), the profiles shown in Figure 4 suggest that the prediction capabilities of cases 6 and 7 are quite similar with minor dissimilarities since the UFM model is based on post-processing of the converged predictions derived from the SFM model [41]. An important observation that can be made from Figure 4 is that the combustion residence time and, consequently, the ability to reach the chemical equilibrium state is influenced by the adopted combustion model (i.e., partially premixed model, SFM or UFM), all of which have an impact on the overall predictions. That is, the chemically active zone where both non-premixed and premixed terms of the reaction rates play a significant role is predicted differently using mixture fraction based models (either partially premixed based or purely non-premixed based model), which can be explained via the formation of CH_2O and OH inside the furnace (See Figure 5 and further explanation below).

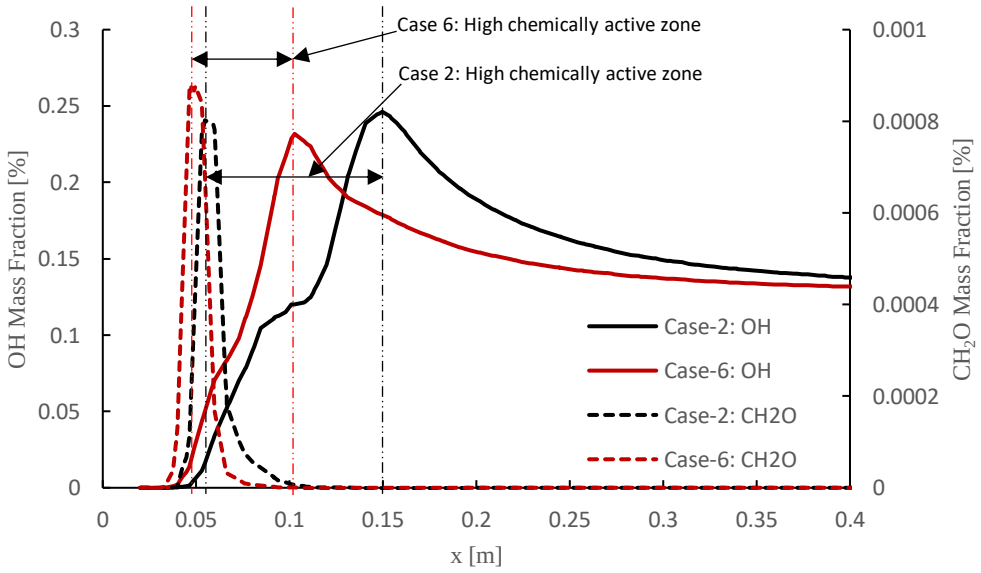

Figure 5: Profiles of CH_2O and OH mole fraction along the centerline of the furnace for cases 2 and 6.

The predictions of CH_2O and OH mass fractions along the centerline of the furnace are shown in Figure 5 for cases 2 and 6. We chose these two cases because both of them adopt SFM (case 2 adopts partially premixed and case 6 adopts non-premixed). Figure 5 shows that for case 6, the formation of formaldehyde (CH_2O) reaches its peak earlier, and OH formation reaches its peak much closer to the bed. It was previously reported that the mass fraction peak of CH_2O occurs in the fuel-rich zone, and that of OH manifests predominantly in the non-premixed reaction zone of a merged flame structure (i.e., transition occurs between non-premixed and premixed flame structure in a partially premixed regime) [103]. The zone between these two peaks (considered a highly chemically reactive zone) is regarded as the transition zone, where the transition between a fuel-rich regime to a purely non-premixed regime might take place, and both non-premixed and premixed regimes may locally affect the structure of the flame [104] [74]. In a previous numerical study on Sandia flame D with predominantly non-premixed characteristics [74], it was shown that both non-premixed and premixed budgets of the wrinkling-EDC combustion model play a significant role in the overall calculation of the chemical reaction rate, which justifies the choice of partially premixed models over purely non-premixed models when even modelling partially premixed regimes having predominantly non-premixed characteristics. The findings of this figure suggest that the choice of the combustion model has an apparent influence on the reaction zone characteristics, where the non-premixed model (case 6) predicts a narrower transition zone (this is discussed in Figure 6 below). This is why the peak temperature of case 6 occurs earlier than case 2 (Figure 3(a)) since the highly chemically active zone is narrowed in case 6, which is also evident by the trend of CO_2 production and O_2 consumption (as a representative of fuel consumption) of case 6 in the same region (see Figure 4(b)). The partially premixed model (case 2), on the other

hand, shows a larger transition zone according to the profiles of CH_2O and OH mass fractions shown in Figure 5.

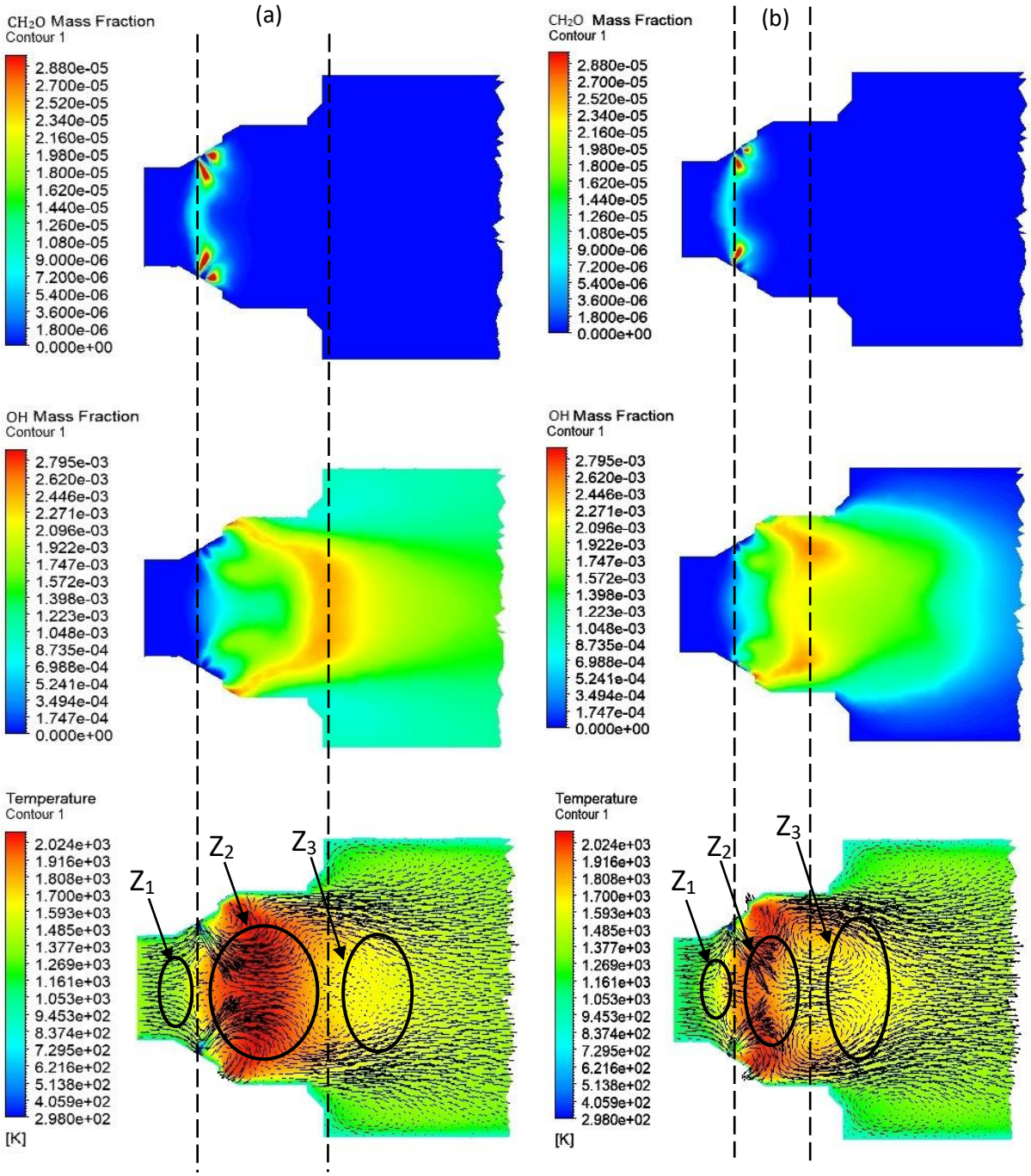

Figure 6. Contours of CH_2O and OH mass fraction and temperature. (a) Partially premixed combustion model (case 2), and (b) Non-premixed model (case 6).

Figure 6 shows 2D contours of CH_2O and *OH* mass fractions and temperature inside the furnace for case 2 (partially premixed model with C equation-SFM, Figure 6(a)), and case 6 (purely non-premixed model with SFM, Figure 6(b)). Zone Z_2, or the transition zone, spans from high local CH_2O concentration to the high local *OH* concentration, which indicates the highly chemically active zone, as discussed before in [74]. This is also evident from the temperature contours where the highest local temperature is stretched within this zone. That is, the temperature drastically rises in this zone due to the higher chemical activities. Figure 6 also reveals the effect of the combustion model on the prediction of the velocity field within the furnace. From the velocity vectors shown in Figure 6 (a) and (b), it is evident that the prediction of velocity vectors by the aforementioned combustion models has a direct influence on the prediction of these zones (i.e., Z_1, Z_2 and Z_3). It is visible from the velocity vectors that both of the combustion models (cases 2 & 6) predict three recirculation zones, which corroborate the findings reported in Farokhi et al. [17]. When compared against the previously shown predicted values of CH_2O and *OH* mass fraction along the centerline of the furnace (Figure 5), it is quite evident that CH_2O and *OH* mass fraction peaks align with the eye of the first and third recirculation zone, respectively. This can also be seen when compared against the contours of CH_2O and *OH* mass fractions. The velocity vectors show that the distance of these two recirculation zones (i.e., Z_1 and Z_3) is influenced by the combustion models (i.e., partially premixed combustion and non-premixed combustion model). Compared to case 2, case 6 predicted a shorter second recirculation zone, resulting in an early prediction of *OH* mass fraction peak. The temperature contours indicate that most of the chemical reactions take place in this second recirculation zone. Due to the influence of the tertiary airflow, with the flow coming out of the zone Z_2, a third recirculation zone (i.e., zone Z_3) is being created behind the high-temperature region and almost after the high *OH* concentration region. As can be seen from the temperature

contours and velocity vectors shown in Figure 6, the choice of partially premixed and purely non-premixed combustion models has a noticeable influence on the prediction of zone Z_3 and its influence on high temperature and transition zone (i.e., zone Z_2). That is, during the recirculation zone Z_3 causes partial recirculation of fresh air injected from tertiary air into the end tip of the transition zone (i.e., zone Z_2), this recirculation appears larger and seems to push more fresh and cold air into the zone Z_2 when using the purely non-premixed model. Thus, one of the reasons for predicting a smaller transition region along with lower high temperature in case 6 might be related to the prediction of a larger recirculation zone Z_3 and consequently higher concentrations of colder inlet air coming inside the transition zone, which is also evident from the higher level of oxygen concentration in the same regions of the furnace (see Figure 4(b)).

5.2 Sensitivity analysis of the boundary conditions

In this study, two different boundary conditions (i.e., BC-1 and BC-2) have been used to evaluate the sensitivity of the predictions of temperature field and species concentrations within the freeboard. BC-1 and BC-2 were used along with the C Equation/UFM-based partially premixed combustion model for cases 3 (BC-1) and 4 (BC-2). Figure 7(a) depicts the temperature profile along the centerline of the furnace as predicted by BC-1 (case 3) and BC-2 (case 4). This figure shows that the predicted peak temperature in the local high-temperature region (i.e., up to $x \approx 0.3\ m$) is clearly influenced by the selected boundary conditions. In this local high-temperature region, BC-1 causes a slightly higher peak temperature (2004K) in case 3 compared to BC-2 (1941 K) in case 4. This slightly higher peak temperature of BC-2 is directly related to the mass fraction of the volatile gases (i.e., CH_4 and $C_6H_{10}O_5$) coming from the bed and also to the lower O_2 concentration in this region of the furnace (see Figure 8(b) and Figure 9) [65].

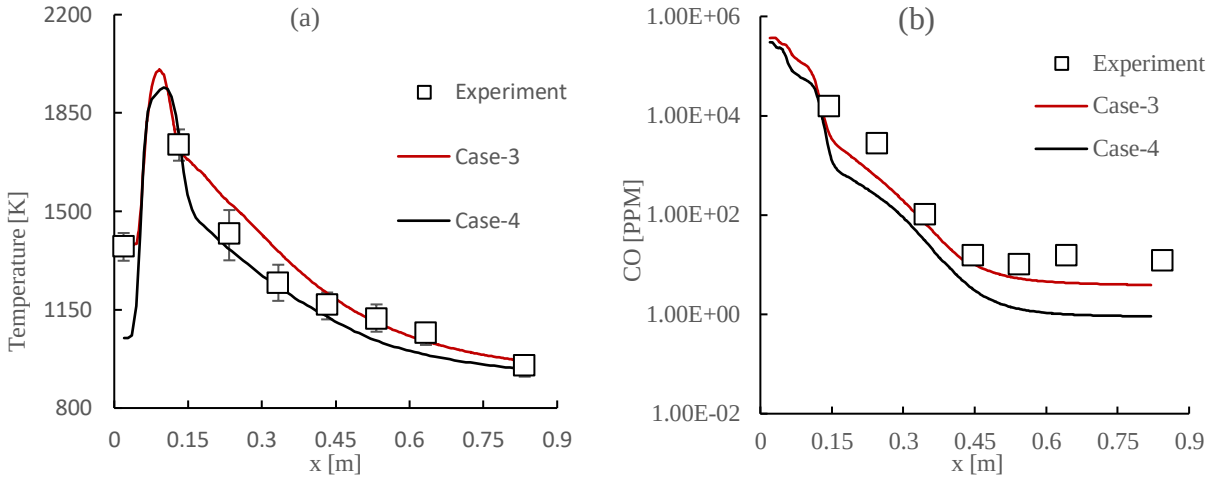

Figure 7. Profiles of (a) temperature and (b) *CO* concentration along the centerline of the furnace for cases 3 & 4.

The influence of BC-1 and BC-2 on the prediction of *CO* can be seen in Figure 7(b). *CO* concentration downstream of the furnace is also influenced by the boundary conditions (i.e., BC-1 or BC-2), especially after the peak temperature region (i.e., after $x \approx 0.15\ m$). Figure 7(b) shows that in both cases 3 and 4, the prediction starts with a higher *CO* concentration in the local high-temperature region that is caused by the enhanced dissociation of CO_2 in that region. Compared to case 3, which uses BC-1, Figure 7(a) shows that the prediction of the temperature profile downstream of the furnace (after the peak temperature region $0.15\ m < x < 0.3\ m$) is lower and also quantitatively closer to the experimental value in case 4. This is due to less fuel-driven species concentration (i.e., CH_4 and $C_6H_{10}O_5$) predicted in case 4 (which uses BC-2), and hence there is less fuel for extracting heat/energy (see Figure 9). On the other hand, when compared to the measurements, case 3 (which uses BC-1) produces a quantitatively better prediction of *CO* concentration than case 4 (which uses BC-2) downstream of the furnace. Nonetheless, both boundary conditions yield predictions that are qualitatively in reasonable agreement with the measurements but with better results in case 3.

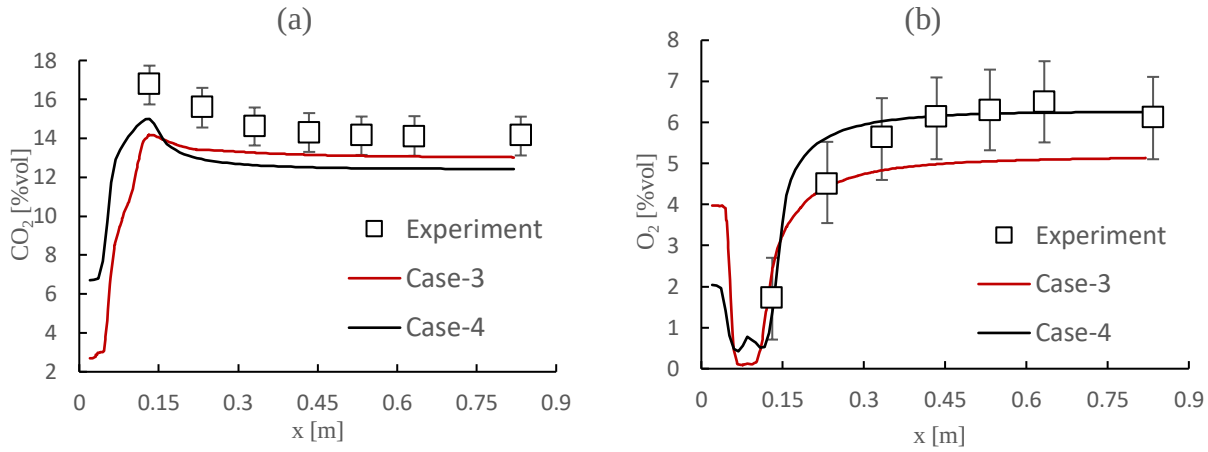

Figure 8. Profiles of (a) CO_2 mole fraction and (b) O_2 mole fraction along the centerline of the furnace for cases 3 & 4.

Figure 8(a) and (b) present the effect of boundary conditions BC-1 and BC-2 on the predictions of CO_2 and O_2 mole fractions along the centerline of the furnace. Both cases 3 and 4 predict a similar trend to the experiments but are quantitatively different. Also, both cases indicate that the overall combustion takes place between zone Z_1 and zone Z_3 (shown in Figure 6), which is caused by the decaying of turbulence downstream of the furnace [17]. This phenomenon causes the establishment of an equilibrium chemistry condition downstream of the furnace and, thereby, a near-equilibrium level of CO_2 and O_2 concentration [17], [41]. Overall, the predictions of case 4 are quantitatively in better agreement with the experiments. That is, the prediction of CO_2 concentration is similar for both cases, although case 3 slightly underpredicts the species in the local peak temperature region (i.e., up to $x \approx 0.15\ m$). The influence of boundary conditions is more prominent in the prediction of O_2 concentration. Figure 8 suggests that, for both cases 3 and 4, the bulk of combustion takes place in the local peak temperature region (i.e., up to $x \approx 0.30\ m$), which causes a lower concentration of O_2 in this region. It can be concluded from Figure 7 and Figure 8 that the selection of bed boundary conditions has a discernible influence on the prediction of temperature field and species concentrations downstream of the furnace (that is, when the

chemical equilibrium condition is established [17]). Both Figure 7 and Figure 8, however, show that the predictions are relatively similar in trend to the measurements using either BC-1 or BC-2 boundary conditions.

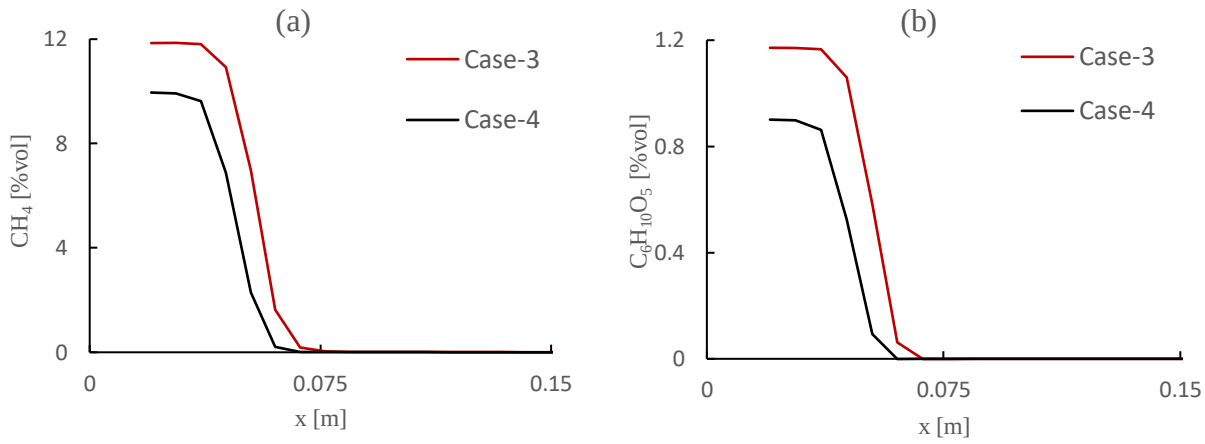

Figure 9. Profiles of the mole fraction of (a) CH_4 and (b) $C_6H_{10}O_5$ along the centerline of the furnace for cases 3 & 4.

The above-discussed results of temperature and species concentration revealed that the numerical predictions are highly dependent on the consumption of the released volatile gases (e.g., CH_4 and $C_6H_{10}O_5$) from the bed. Figure 9(a) and (b) depict the concentration and consumption of, respectively, CH_4 and $C_6H_{10}O_5$, in both cases 3 and 4 along the centerline of the furnace. Figure 9 shows that the supplied amount of combustible volatile gases in the freeboard is predicted to be higher in case 3, which yields a higher release of energy. On the other hand, considering the conversion of energy and mass, it appears that a higher portion of the energy is released within the bed in case 4, which is also evident from the higher closer-to-bed temperature profile in case 4 (see Figure 7(a)), higher production of combustion major products (i.e., CO_2) and higher consumption of O_2 in the vicinity of the bed for case 4 (see Figure 8(a) and (b)). In agreement with published literature (e.g., [17]), this figure distinctly indicates that the combustion process and

volatile gas consumption cannot be predicted adequately near the bed due to very weak turbulence and lower strain rates.

5.3 Partially premixed model versus EDC/Flamelet model

The performance of the partially premixed combustion model has been compared with EDC/Flamelet model in this section. The predicted temperature profiles and the concentration of *CO* along the centerline of the furnace are shown in Figure 10(a) and (b), respectively. Overall, the temperature profile appears to be less influenced by the combustion model. All predicted temperature profiles compare reasonably well with the measurements, though the partially premixed combustion model (i.e., cases 4 and 4b) insignificantly under-predicts the temperature compared to EDC/FLamelet model.

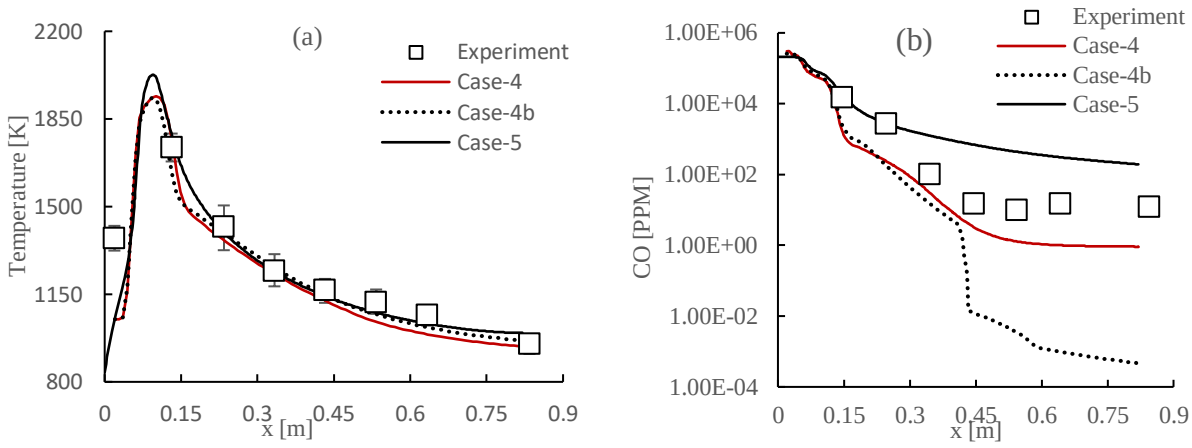

Figure 10. Profiles of (a) temperature and (b) *CO* concentration along the centerline of the furnace for cases 4 & 5.

On the other hand, it is evident in Figure 10(b) that the adopted combustion model has a significant influence on the prediction of slow-forming species (i.e., *CO*) in line with published literature [17]. Compared to the measurements, case 4b predicts *CO* concentration reasonably well until after the mid of the furnace (i.e., up to $x \approx 0.45\ m$, where the chemical equilibrium condition is believed to start taking place), after which SFM starts to underpredict the concentration of *CO* mole fraction.

Case 5 (EDC/Flamelet model) predicts *CO* concentration reasonably well in the local high-temperature region (i.e., up to $x \approx 0.30\ m$) but then over-predicts it downstream of the furnace in the chemical equilibrium region. On the other hand, the C equation and UFM-based partially premixed model (i.e., case 4) appear to be reasonably capable of predicting *CO* concentration throughout the furnace. That is, the prediction of *CO* concentration is in good agreement with the measurements at the onset of the local peak temperature region (i.e., up to $x \approx 0.15\ m$) and then slightly drifts below the measurement downstream of the furnace. Overall, compared to the experiments, this model (case 4) produces quantitatively better predictions than the EDC/Flamelet model.

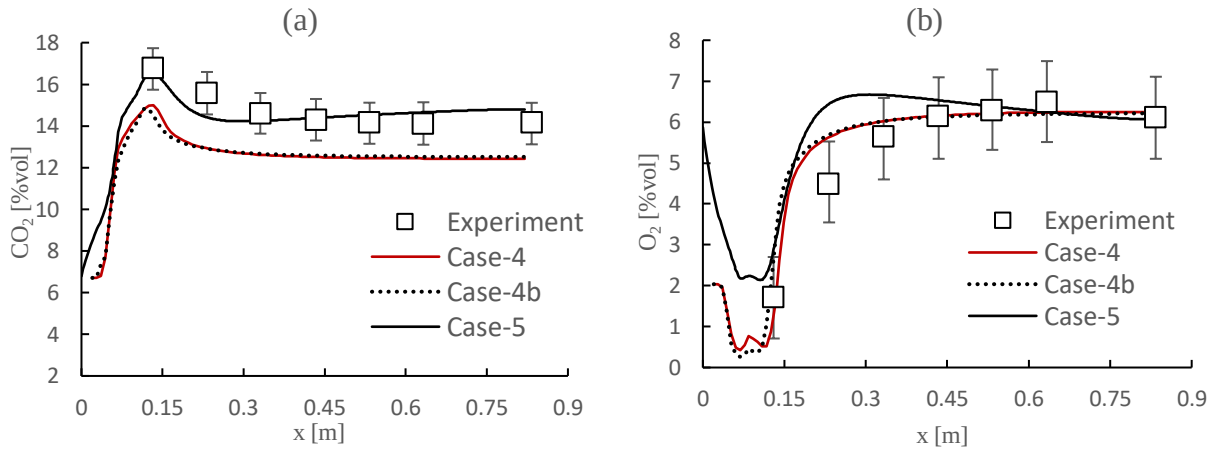

Figure 11. Profiles of mole fraction of (a) CO_2 and (b) O_2 along the centerline of the furnace for cases 4 & 5.

The influence of the partially premixed model and EDC/Flamelet model on the prediction of CO_2 and O_2 mole fractions along the centerline of the furnace is depicted in Figure 11(a) and (b). The predictions of the three cases (i.e., cases 4, 4b & 5) show almost similar trends/profiles and compare well with the experiments. One of the reasons for the underprediction of CO_2 mole fraction in the local high-temperature region by cases 4 and 4b might be related to the enhanced

dissociation of CO_2 [102], which also causes the prediction of higher CO concentration in the same region. CO_2 prediction is also associated with the prediction of temperature. Underprediction in the case of temperature can lead to CO_2 underprediction. Although in the current scenario, this phenomenon can be eliminated as the presented data in Figure 10(a) clearly indicates that the prediction of temperature throughout the furnace is within the error limit. The partially premixed model (i.e., cases 4 and 4b) underpredicts the concentration of CO_2. On the contrary, compared EDC/Flamelet model (case 5), the partially premixed model's prediction of O_2 concentration is quantitatively in better agreement with the measurements. However, moving farther downstream of the furnace, the predicted O_2 mole fraction by both models is quite similar.

Chapter 6 CONCLUSIONS AND RECOMMENDATIONS

6.1 Concluding Remarks

The prediction capability of partially premixed combustion models and the effect of the adopted premixed (i.e., extended coherent flame model and C-equation) and non-premixed (i.e., SFM and UFM) models were examined in this study. In addition, another comparison was conducted to examine the capability of partially premixed mixture fraction-based combustion models against a recently developed EDC/Flamelet hybrid model. The main concluding remarks of this research are summarized as follows:

i. The study revealed that, compared with published experimental data, partially premixed models are capable of producing acceptable predictions. The study revealed that the prediction ability of the UFM-based partially premixed model surpasses that of its SFM-based partially premixed model counterpart, especially in the case of slow-forming species. These conclusions were made on the basis of the temperature field along with major and minor species concentrations.

ii. The prediction ability of partially premixed combustion models (i.e., extended coherent flame model/SFM based, C-equation/SFM based and C-equation/UFM based) was tested in this study, and the results were compared against published predictions of other combustion models (i.e., EDC/Flamelet hybrid, purely non-premixed SFM and UFM combustion models). The results revealed that all investigated partially premixed combustion models produce better predictions than EDC/Flamelet hybrid, purely non-premixed SFM and UFM combustion models, especially for slow-forming CO concentration. This is especially the case when adopting a UFM-based partially premixed model, where the predictions of both velocity and temperature fields were found sensitive

to the adopted combustion model. For instance, compared to the purely non-premixed SFM combustion model, the partially premixed model predicts a wider high chemically reactive zone which expands more downstream of the furnace as a result of a smaller recirculation of cold air within the high temperature/chemically reactive zone that results in higher temperature distribution in the local high-temperature region (i.e., up to $x \approx 0.3\ m$).

iii. Amongst all examined partially premixed modes, the C-equation/UFM-based partially premixed model has the best results in the predictions of the slow-forming chemistry species (i.e., *CO*) in addition to its adequate prediction ability of the temperature field and major and minor species.

6.2 Recommendations

While there is a good progress in developing reliable numerical modelling of biomass combustion, there is still a need for further research. A few research directions are provided below.

i. NO_x calculation in the postprocessing is not compatible with partially premixed combustion models. A kinetic mechanism for calculating NO_x should be developed, which is expected to enhance the prediction ability of partially premixed models.

ii. A new hybrid combustion model (i.e., wrinkling-EDC) was recently proposed by Farokhi and Birouk [74], [105] to overcome the standard EDC model's limitations in predicting both premixed and non-premixed combustion regimes. Since combustion inside a grate-firing biomass furnace consists of different combustion regimes (i.e., non-premixed, partially premixed and premixed) [33]–[35], it is useful to assess the ability of this model for the simulation of this multi-regime combustion. This study can also be coupled with the introduction of a pre-calculated flamelet approach in order to reduce the computational cost.

References:

[1] B. P, "Electricity - BP Statistical Review of World Energy 2018," *https//www. bp. com/en/global/corporate/energy-economics/statistical-review-of-world-energy. Sustain.*, vol. 10, no. 3195, pp. 1–4, 2018.

[2] J. Floyd, S. Alexander, M. Lenzen, P. Moriarty, G. Palmer, S. Chandra-Shekeran, B. Foran, and L. Keyßer, "Energy descent as a post-carbon transition scenario: How 'knowledge humility' reshapes energy futures for post-normal times," *Futures*, vol. 122, p. 102565, Sep. 2020, doi: 10.1016/J.FUTURES.2020.102565.

[3] R. W. Bentley, "Global oil and gas depletion: An overview," *Energy Policy*, vol. 30, no. 3, pp. 189–205, Feb. 2002, doi: 10.1016/S0301-4215(01)00144-6.

[4] U. Bardi, "The mineral economy: A model for the shape of oil production curves," *Energy Policy*, vol. 33, no. 1, pp. 53–61, Jan. 2005, doi: 10.1016/S0301-4215(03)00197-6.

[5] M. Momeni, "Fundamental Study of Single Biomass Particle Combustion," Department of Energy Technology, Aalborg University, 2013. [Online]. Available: https://vbn.aau.dk/en/publications/fundamental-study-of-single-biomass-particle-combustion

[6] T. Klason and X. S. Bai, "Computational study of the combustion process and NO formation in a small-scale wood pellet furnace," *Fuel*, vol. 86, no. 10–11, pp. 1465–1474, Jul. 2007, doi: 10.1016/j.fuel.2006.11.022.

[7] T. Klason, "Modelling of Biomass Combustion in Furnaces," Ph.D. thesis, Lund Institute of Technology, 2006. doi: 10.13140/RG.2.2.15695.38568.

[8] H. Lu, E. Ip, J. Scott, P. Foster, M. Vickers, and L. L. Baxter, "Effects of particle shape and size on devolatilization of biomass particle," *Fuel*, vol. 89, no. 5, pp. 1156–1168, May 2010, doi: 10.1016/j.fuel.2008.10.023.

[9] S. Sukumaran and S. C. Kong, "Modeling fuel NOx formation from combustion of biomass-derived producer gas in a large-scale burner," *Combust. Flame*, vol. 160, no. 10, pp. 2159–2168, Oct. 2013, doi: 10.1016/j.combustflame.2013.04.020.

[10] "Department of Energy." https://www.energy.gov/energybasics/articles/biomass/resource-basics (accessed Sep. 21, 2020).

[11] A. Demirbaş, "Biomass resource facilities and biomass conversion processing for fuels and chemicals," *Energy Convers. Manag.*, vol. 42, no. 11, pp. 1357–1378, Jul. 2001, doi: 10.1016/S0196-8904(00)00137-0.

[12] S. van Loo and J. Koppejan, *The handbook of biomass combustion and co-firing*. 2012. doi: 10.4324/9781849773041.

[13] M. Buchmayr, J. Gruber, M. Hargassner, and C. Hochenauer, "A computationally inexpensive CFD approach for small-scale biomass burners equipped with enhanced air staging," *Energy Convers. Manag.*, vol. 115, pp. 32–42, May 2016, doi: 10.1016/j.enconman.2016.02.038.

[14] J. Andersen, "Experimental and CFD investigation of gas phase freeboard combustion," Ph. D. thesis, Technical University of Denmark, 2009.

[15] C. Yin, L. A. Rosendahl, and S. K. Kær, "Grate-firing of biomass for heat and power production," *Prog. Energy Combust. Sci.*, vol. 34, no. 6, pp. 725–754, Dec. 2008, doi:

10.1016/j.pecs.2008.05.002.

[16] M. Farokhi, “Numerical study of biomass combustion of a grate-firing furnace with emphasis on gas-phase combustion modeling,” Ph. D. thesis, University of Manitoba, 2018.

[17] M. Farokhi, M. Birouk, and F. Tabet, “A computational study of a small-scale biomass burner: The influence of chemistry, turbulence and combustion sub-models,” *Energy Convers. Manag.*, vol. 143, pp. 203–217, Jul. 2017, doi: https://doi.org/10.1016/j.enconman.2017.03.086.

[18] H. A. J. A. Van Kuijk, R. J. M. Bastiaans, J. A. Van Oijen, and L. P. H. De Goey, “Grate furnace combustion: A submodel for the solid fuel layer,” *Int. J. Multiscale Comput. Eng.*, vol. 6, no. 1, pp. 103–111, 2008, doi: 10.1615/IntJMultCompEng.v6.i1.90.

[19] T. Jurena, “Numerical modelling of grate combustion,” *Brno Univ. Technol. Brno*, 2012.

[20] M. Farokhi and M. Birouk, “Application of Eddy Dissipation Concept for Modeling Biomass Combustion, Part 2: Gas-Phase Combustion Modeling of a Small-Scale Fixed Bed Furnace,” *Energy & Fuels*, vol. 30, pp. 10800–10808, 2016, doi: 10.1021/acs.energyfuels.6b01947.

[21] J. Chaney, H. Liu, and J. Li, “An overview of CFD modelling of small-scale fixed-bed biomass pellet boilers with preliminary results from a simplified approach,” *Energy Convers. Manag.*, vol. 63, pp. 149–156, 2012, doi: 10.1016/j.enconman.2012.01.036.

[22] D. Eskilsson, M. Ronnback, J. Samuelsson, and C. Tullin, “Optimisation of efficiency and emissions in pellet burners,” *Biomass and Bioenergy*, vol. 27, pp. 541–546, 2004, doi: 10.1016/j.biombioe.2003.09.008.

[23] C. Yin, L. Rosendahl, S. K. Kær, S. Clausen, S. L. Hvid, and T. Hiller, "Mathematical modeling and experimental study of biomass combustion in a thermal 108 MW grate-fired boiler," *Energy and Fuels*, vol. 22, no. 2, pp. 1380–1390, 2008, doi: 10.1021/ef700689r.

[24] J. Porteiro, J. Collazo, D. Patiño, E. Granada, J. C. M. Gonzalez, and J. L. Míguez, "Numerical modeling of a biomass pellet domestic boiler," *Energy and Fuels*, vol. 23, no. 2, pp. 1067–1075, 2009, doi: 10.1021/ef8008458.

[25] X. Zhang, Q. Chen, R. Bradford, V. Sharifi, and J. Swithenbank, "Experimental investigation and mathematical modelling of wood combustion in a moving grate boiler," *Fuel Process. Technol.*, vol. 91, no. 11, pp. 1491–1499, Nov. 2010, doi: 10.1016/j.fuproc.2010.05.026.

[26] Z. Taban, "Bed Modeling of a Biomass Grate-Firing Furnace : A Numerical Study," Master's thesis, University of Manitoba, 2018.

[27] F. Scala, *Fluidized Bed Technologies for Near-Zero Emission Combustion and Gasification*. Elsevier, 2013.

[28] B. F. Magnussen and B. H. Hjertager, "On mathematical modeling of turbulent combustion with special emphasis on soot formation and combustion," *Symp. Combust.*, vol. 16, no. 1, pp. 719–729, Jan. 1977, doi: 10.1016/S0082-0784(77)80366-4.

[29] B. F. MAGNUSSEN, "On the structure of turbulence and a generalized eddy dissipation concept for chemical reaction in turbulent flow," *19th AIAA Aerosp. Sci. Meet. St. Louis, Missouri*, p. 42, 1981, doi: 10.2514/6.1981-42.

[30] A. Shiehnejadhesar, R. Scharler, R. Mehrabian, and I. Obernberger, "Development and

validation of CFD models for gas phase reactions in biomass grate furnaces considering gas streak formation above the packed bed," *Fuel Process. Technol.*, vol. 139, pp. 142–158, 2015, doi: 10.1016/j.fuproc.2015.07.029.

[31] M. Farokhi and M. Birouk, "Application of Eddy Dissipation Concept for Modeling Biomass Combustion, Part 1: Assessment of the Model Coefficients," *Energy & Fuels*, vol. 30, pp. 10789–10799, 2016, doi: 10.1021/acs.energyfuels.6b01947.

[32] B. A. Albrecht, S. Zahirovic, R. J. M. Bastiaans, J. A. van Oijen, and L. P. H. de Goey, "A premixed flamelet-PDF model for biomass combustion in a grate furnace," *Energy and Fuels*, vol. 22, no. 3, pp. 1570–1580, May 2008, doi: 10.1021/ef7007562.

[33] A. Shiehnejadhesar, R. Mehrabian, C. Hochenauer, and R. Scharler, "The virtual biomass grate furnace-an overall CFD model for biomass combustion plants," *Energy Procedia*, vol. 120, pp. 516–523, 2017, doi: 10.1016/j.egypro.2017.07.189.

[34] A. Shiehnejadhesar, R. Mehrabian, R. Scharler, G. M. Goldin, and I. Obernberger, "Development of a gas phase combustion model suitable for low and high turbulence conditions," *Fuel*, vol. 126, no. 2014, pp. 177–187, 2014, doi: 10.1016/j.fuel.2014.02.040.

[35] A. Shiehnejadhesar, R. Mehrabian, R. Scharler, and I. Obernberger, "Development of a streak formation model for an improved prediction of gas phase combustion in biomass grate furnaces," in *Proc. of 10th European Conference on Industrial Furnaces and Boilers INFUB*, 2015, no. April, pp. 1–15.

[36] T. Klason, X. S. Bai, M. Bahador, T. K. Nilsson, and B. Sundén, "Investigation of radiative heat transfer in fixed bed biomass furnaces," *Fuel*, vol. 87, no. 10–11, pp. 2141–2153, 2008, doi: 10.1016/j.fuel.2007.11.016.

[37] J. Labahn, “Investigation of Conditional Source-term Estimation Approach to Modelling MILD Combustion,” Ph. D. thesis, University of Waterloo, 2016.

[38] N. Peters, *Turbulent combustion*. Cambridge university press, 2000. doi: 10.1017/CBO9780511612701.

[39] A. Y. Klimenko and R. W. Bilger, “Conditional moment closure for turbulent combustion,” *Prog. Energy Combust. Sci.*, vol. 25, no. 6, pp. 595–687, Dec. 1999, doi: 10.1016/S0360-1285(99)00006-4.

[40] J. O. Hinze, “Turbulence. McGraw-Hill Publishing Co,” *New York*, 1975.

[41] ANSYS, “ANSYS Fluent Theory Guide, Release 15.0,” *Ansys*. [Online]. Available: http://www.afs.enea.it/project/neptunius/docs/fluent/html/th/main_pre.htm

[42] D. F. Fletcher, B. S. Haynes, F. C. Christo, and S. D. Joseph, “A CFD based combustion model of an entrained flow biomass gasifier,” *Appl. Math. Model.*, vol. 24, no. 3, pp. 165–182, 2000, doi: 10.1016/S0307-904X(99)00025-6.

[43] D. F. Fletcher, B. S. Haynes, J. Chen, and S. D. Joseph, “Computational fluid dynamics modelling of an entrained flow biomass gasifier,” *Appl. Math. Model.*, vol. 22, no. 10, pp. 747–757, 1998, doi: 10.1016/S0307-904X(98)10025-2.

[44] H. Knaus, S. Richter, S. Unterberger, U. Schnell, H. Maier, and K. R. G. Hein, “On the application of different turbulence models for the computation of fuid flow and combustion processes in small scale wood heaters,” *Exp. Therm. Fluid Sci.*, vol. 21, no. 1, pp. 99–108, 2000, doi: https://doi.org/10.1016/S0894-1777(99)00059-X.

[45] B. E. Launder and D. B. Spalding, “Lectures in mathematical models of turbulence,” 1972.

[46] V. Yakhot, “Renormalization group modeling and turbulence simulations,” in *International Conference on Near-Wall Turbulent Flows, Tempe, Arizona*, 1993, pp. 1031–1046.

[47] T.-H. Shih, W. W. Liou, A. Shabbir, Z. Yang, and J. Zhu, “A new k-ϵ eddy viscosity model for high reynolds number turbulent flows,” *Comput. Fluids*, vol. 24, no. 3, pp. 227–238, 1995, doi: https://doi.org/10.1016/0045-7930(94)00032-T.

[48] F. Tabet, V. Fichet, and P. Plion, “A comprehensive CFD based model for domestic biomass heating systems,” *J. Energy Inst.*, vol. 89, no. 2, pp. 199–214, 2016, doi: https://doi.org/10.1016/j.joei.2015.02.003.

[49] J. Collazo, J. Porteiro, J. L. Míguez, E. Granada, and M. A. Gómez, “Numerical simulation of a small-scale biomass boiler,” *Energy Convers. Manag.*, vol. 64, pp. 87–96, 2012, doi: 10.1016/j.enconman.2012.05.020.

[50] Y. Wang and L. Yan, “CFD Studies on Biomass Thermochemical Conversion,” *Int. J. Mol. Sci.*, vol. 9, no. 6, pp. 1108–1130, 2008, doi: 10.3390/ijms9061108.

[51] A. Hölzer and M. Sommerfeld, “New simple correlation formula for the drag coefficient of non-spherical particles,” *Powder Technol.*, vol. 184, no. 3, pp. 361–365, 2008, doi: https://doi.org/10.1016/j.powtec.2007.08.021.

[52] D. J. O. Ferreira, J. H. Sosa Arnao, B. C. Moreira, L. P. Rangel, and S. W. Park, “The impact of radiation in the gas combustion model for sugarcane bagasse grate boiler,” *Brazilian J. Chem. Eng.*, vol. 33, no. 3, pp. 617–626, Jul. 2016, doi: 10.1590/0104-6632.20160333s20150143.

[53] A. De, E. Oldenhof, P. Sathiah, and D. Roekaerts, “Numerical simulation of Delft-Jet-in-

Hot-Coflow (DJHC) flames using the eddy dissipation concept model for turbulence-chemistry interaction," *Flow, Turbul. Combust.*, vol. 87, no. 4, pp. 537–567, Dec. 2011, doi: 10.1007/s10494-011-9337-0.

[54] M. Rehm, P. Seifert, and B. Meyer, "Theoretical and numerical investigation on the EDC-model for turbulence--chemistry interaction at gasification conditions," *Comput. Chem. Eng.*, vol. 33, no. 2, pp. 402–407, 2009, doi: 10.1016/j.compchemeng.2008.11.006.

[55] A. Parente, M. R. Malik, F. Contino, A. Cuoci, and B. B. Dally, "Extension of the Eddy Dissipation Concept for turbulence/chemistry interactions to MILD combustion," *Fuel*, vol. 163, pp. 98–111, 2016, doi: 10.1016/j.fuel.2015.09.020.

[56] I. R. Gran, M. C. Melaaen, and B. F. Magnussen, "Numerical simulation of local extinction effects in turbulent combustor flows of methane and air," *Combust. Inst.*, vol. 25, no. 1, pp. 1283–1291, Jan. 1994, doi: 10.1016/S0082-0784(06)80769-1.

[57] M. J. Evans, C. Petre, P. R. Medwell, and A. Parente, "Generalisation of the eddy-dissipation concept for jet flames with low turbulence and low Damköhler number," *Proc. Combust. Inst.*, vol. 37, no. 4, pp. 4497–4505, 2019, [Online]. Available: http://dx.doi.org/10.1016/j.proci.2018.06.017

[58] M. Lewandowski, A. Parente, and J. Pozorski, "Generalised Eddy Dissipation Concept for MILD combustion regime at low local Reynolds and Damköhler numbers. Part 1: Model framework development," *Fuel*, vol. 278, p. 117743, 2020, [Online]. Available: http://dx.doi.org/10.1016/j.fuel.2020.117743

[59] H. Bao, "Development and validation of a new Eddy Dissipation Concept (EDC) model for MILD combustion," Master's Thesis, Delft University of Technology, 2017. [Online].

Available: https://resolver.tudelft.nl/uuid:45fdb951-408f-404f-8b9a-71f2eda6540b

[60] N. Romero-Anton, X. Huang, H. Bao, K. Martin-Eskudero, E. Salazar-Herran, and D. Roekaerts, "New extended eddy dissipation concept model for flameless combustion in furnaces," *Combust. Flame*, vol. 220, pp. 49–62, 2020, [Online]. Available: http://dx.doi.org/10.1016/j.combustflame.2020.06.025

[61] E. E. Fordoei, K. Mazaheri, and A. Mohammadpour, "Numerical study on the heat transfer characteristics, flame structure, and pollutants emission in the MILD methane-air, oxygen-enriched and oxy-methane combustion," *Energy*, vol. 218, p. 119524, 2021, [Online]. Available: http://dx.doi.org/10.1016/j.energy.2020.119524

[62] I. S. Ertesvåg, "Scrutinizing proposed extensions to the Eddy Dissipation Concept (EDC) at low turbulence Reynolds numbers and low Damköhler numbers," *Fuel*, vol. 309, p. 122032, 2022.

[63] M. Farokhi and M. Birouk, "A new EDC approach for modeling turbulence/chemistry interaction of the gas-phase of biomass combustion," *Fuel*, vol. 220, pp. 420–436, 2018, doi: 10.1016/j.fuel.2018.01.125.

[64] R. Prieler, M. Demuth, D. Spoljaric, and C. Hochenauer, "Numerical investigation of the steady flamelet approach under different combustion environments," *Fuel*, vol. 140, pp. 731–743, 2015, doi: 10.1016/j.fuel.2014.10.006.

[65] M. Farokhi and M. Birouk, "A hybrid EDC/Flamelet approach for modelling biomass combustion of grate-firing furnace," *Combust. Theory Model.*, vol. 23, no. 4, pp. 716–747, 2019, doi: 10.1080/13647830.2019.1587177.

[66] N. Peters, “Laminar diffusion flamelet models in non-premixed turbulent combustion,” *Prog. energy Combust. Sci.*, vol. 10, no. 3, pp. 319–339, 1984.

[67] H. Pitsch, M. Chen, and N. Peters, “Unsteady flamelet modeling of turbulent hydrogen-air diffusion flames,” in *Combustion Institute*, 1998, vol. 27, no. 1, pp. 1057–1064.

[68] S. Zahirović, R. Scharler, P. Kilpinen, and I. Obernberger, “Validation of flow simulation and gas combustion sub-models for the CFD-based prediction of NOx formation in biomass grate furnaces,” *Combust. Theory Model.*, vol. 15, no. 1, pp. 61–87, 2011, doi: 10.1080/13647830.2010.524312.

[69] D. Borello, P. Venturini, F. Rispoli, and S. G. Z. Rafael, “Prediction of multiphase combustion and ash deposition within a biomass furnace,” *Appl. Energy*, vol. 101, pp. 413–422, 2012, doi: 10.1016/j.applthermaleng.2011.08.030.

[70] A. C. Benim and K. J. Syed, “Laminar flamelet modelling of turbulent premixed combustion,” *Appl. Math. Model.*, vol. 22, no. 1–2, pp. 113–136, 1998, doi: 10.1016/S0307-904X(98)00012-2.

[71] R. Yadav, P. Nakod, and P. Rajeshirke, “NO prediction in turbulent diffusion flame using multiple unsteady laminar flamelet modeling,” *J. Eng. Gas Turbines Power*, vol. 136, no. 10, 2014, doi: 10.1115/1.4026801.

[72] A. Heyl and H. Bockhorn, “Flamelet modeling of NO formation in laminar and turbulent diffusion flames,” *Chemosphere*, vol. 42, no. 5–7, pp. 449–462, 2001.

[73] J. Aminian, C. Galletti, and L. Tognotti, “Extended EDC local extinction model accounting finite-rate chemistry for MILD combustion,” *Fuel*, vol. 165, pp. 123–133, 2016, doi:

10.1016/j.fuel.2015.10.041.

[74] M. Farokhi and M. Birouk, “A comprehensive assessment of fractal wrinkling/eddy dissipation based combustion model for simulating conventional turbulent premixed and non-premixed flames,” *Combust. Theory Model.*, vol. 25, no. 2, pp. 235–268, 2021, doi: 10.1080/13647830.2020.1854349.

[75] C. Xiao, M. Omidi, A. Surendar, A. Alizadeh, D. O. Bokov, Binyamin, and D. Toghraie, “Simulation of Combustion Flow of Methane Gas in a Premixed Low-Swirl Burner using a Partially Premixed Combustion Model,” *J. Therm. Sci. 2022*, vol. 31, pp. 1–19, May 2022, doi: 10.1007/S11630-022-1611-Z.

[76] E. Ranzi, A. Cuoci, T. Faravelli, A. Frassoldati, G. Migliavacca, S. Pierucci, and S. Sommariva, “Chemical kinetics of biomass pyrolysis,” *Energy & Fuels*, vol. 22, no. 6, pp. 4292–4300, 2008, doi: 10.1021/ef800551t.

[77] M. Corbetta, A. Frassoldati, H. Bennadji, K. Smith, M. J. Serapiglia, G. Gauthier, T. Melkior, E. Ranzi, and E. M. Fisher, “Pyrolysis of centimeter-scale woody biomass particles: kinetic modeling and experimental validation,” *Energy & Fuels*, vol. 28, no. 6, pp. 3884–3898, 2014, doi: 10.1021/ef500525v.

[78] H. Grotjans and F. Menter, “Wall functions for industrial applications,” *Proc. Comput. Fluid Dyn. ECCOMAS, Chichester, UK.*, 1998.

[79] B. A. Kader, “Temperature and concentration profiles in fully turbulent boundary layers,” *Int. J. Heat Mass Transf.*, vol. 24, no. 9, pp. 154–1544, Sep. 1981, doi: 10.1016/0017-9310(81)90220-9.

[80] M. F. Modest and S. Mazumder, *Radiative Heat Transfer*. Academic press, 2021.

[81] N. Selçuk and N. Kayakol, "Evaluation of discrete ordinates method for radiative transfer in rectangular furnaces," *Int. J. Heat Mass Transf.*, vol. 40, no. 2, pp. 213–222, 1997, doi: https://doi.org/10.1016/0017-9310(96)00139-1.

[82] A. Coppalle and P. Vervisch, "The total emissivities of high-temperature flames," *Combust. Flame*, vol. 49, no. 1, pp. 101–108, 1983, doi: https://doi.org/10.1016/0010-2180(83)90154-2.

[83] T. F. Smith, Z. F. Shen, and J. N. Friedman, "Evaluation of Coefficients for the Weighted Sum of Gray Gases Model," *J. Heat Transfer*, vol. 104(4), no. 4, pp. 602–608, 1982, doi: 10.1115/1.3245174.

[84] R. Mehrabian, R. Scharler, A. Weissinger, and I. Obernberger, "Optimisation of biomass grate furnaces with a new 3D packed bed combustion model-on example of a small-scale underfeed stoker furnace," in *Proceedings of the 18th European biomass conference, Lyon, France*, 2010, pp. 1175–1183.

[85] M. A. Gómez, J. Porteiro, D. Patiño, and J. L. Míguez, "CFD modelling of thermal conversion and packed bed compaction in biomass combustion," *Fuel*, vol. 117, pp. 716–732, 2014, doi: https://doi.org/10.1016/j.fuel.2013.08.078.

[86] H. Khodaei, Y. M. Al-Abdeli, F. Guzzomi, and G. H. Yeoh, "An overview of processes and considerations in the modelling of fixed-bed biomass combustion," *Energy (Oxford)*, vol. 88, pp. 946–972, Aug. 2015, doi: https://doi.org/10.1016/j.energy.2015.05.099.

[87] R. S. Miller, K. Harstad, and J. Bellan, "Evaluation of equilibrium and non-equilibrium

evaporation models for many-droplet gas-liquid flow simulations," *Int. J. Multiph. Flow*, vol. 24, no. 6, pp. 1025–1055, 1998, doi: https://doi.org/10.1016/S0301-9322(98)00028-7.

[88] W. E. Ranz and W. R. Marshall, "Vaporation from drops, Part I," *Chem. Eng. Prog*, vol. 48, no. 3, pp. 141–146, 1952.

[89] S. S. Sazhin, "Advanced models of fuel droplet heating and evaporation," *Prog. Energy Combust. Sci.*, vol. 32, no. 2, pp. 162–214, 2006, doi: https://doi.org/10.1016/j.pecs.2005.11.001.

[90] E. Girgis and W. L. H. Hallett, "Wood combustion in an overfeed packed bed, including detailed measurements within the bed," *Energy & Fuels*, vol. 24, no. 3, pp. 1584–1591, 2010, doi: https://doi.org/10.1021/ef901206d.

[91] R. Mehrabian, S. Zahirovic, R. Scharler, I. Obernberger, S. Kleditzsch, S. Wirtz, V. Scherer, H. Lu, and L. L. Baxter, "A CFD model for thermal conversion of thermally thick biomass particles," *Fuel Process. Technol.*, vol. 95, pp. 96–108, Mar. 2012, doi: https://doi.org/10.1016/j.fuproc.2011.11.021.

[92] H. Fatehi and X. S. Bai, "A comprehensive mathematical model for biomass combustion," *Combust. Sci. Technol.*, vol. 186, no. 4–5, pp. 574–593, May 2014, doi: https://doi.org/10.1080/00102202.2014.883255.

[93] S. K. Kær, "Numerical investigation of ash deposition in straw-fired boilers: using CFD as the framework for slagging and fouling predictions," Institut for Energiteknik, Aalborg Universitet, 2001.

[94] K. M. Bryden and K. W. Ragland, "Numerical Modeling of a Deep, Fixed Bed Combustor,"

Energy & Fuels, vol. 10, no. 2, pp. 269–275, Mar. 1996, doi: https://doi.org/10.1021/ef950193p.

[95] H. Wiinikka, "High Temperature Aerosol Formation and Emission Minimisation during Combustion of Wood Pellets," Ph. D. thesis, Lulea University of Technology, Lulea, Sweden, 2005.

[96] S. Patronelli, M. Antonelli, L. Tognotti, and C. Galletti, "Combustion of wood-chips in a small-scale fixed-bed boiler: Validation of the numerical model through in-flame measurements," *Fuel*, vol. 221, pp. 128–137, 2018, doi: https://doi.org/10.1016/j.fuel.2018.02.083.

[97] M. D. Emami and A. Eshghinejad Fard, "Laminar flamelet modeling of a turbulent CH 4/H 2/N 2 jet diffusion flame using artificial neural networks," *Appl. Math. Model.*, vol. 36, no. 5, pp. 2082–2093, 2012, doi: 10.1016/j.apm.2011.08.012.

[98] D. C. Haworth, M. C. Drake, S. B. Pope, and R. J. Blint, "The importance of time-dependent flame structures in stretched laminar flamelet models for turbulent jet diffusion flames," in *Combustion Institute*, 1988, vol. 22, no. 1, pp. 589–597.

[99] D. Veynante and L. Vervisch, "Turbulent combustion modeling," *Prog. Energy Combust. Sci.*, vol. 28, no. 3, pp. 193–266, Mar. 2002, doi: 10.1016/S0360-1285(01)00017-X.

[100] B. Lilleberg, D. Christ, I. S. Ertesvåg, K. E. Rian, and R. Kneer, "Numerical Simulation with an Extinction Database for Use with the Eddy Dissipation Concept for Turbulent Combustion," *Flow, Turbul. Combust. 2013 912*, vol. 91, no. 2, pp. 319–346, May 2013, doi: 10.1007/S10494-013-9463-Y.

[101] M. Farokhi and M. Birouk, “Modeling of the gas-phase combustion of a grate-firing biomass furnace using an extended approach of Eddy Dissipation Concept,” *Fuel*, vol. 227, pp. 412–423, Sep. 2018, doi: 10.1016/J.FUEL.2018.04.102.

[102] A. H. Al-Abbas and J. Naser, “Effect of Chemical Reaction Mechanisms and NOx Modeling on Air-Fired and Oxy-Fuel Combustion of Lignite in a 100-kW Furnace,” *Energy and Fuels*, vol. 26, no. 6, pp. 3329–3348, Jun. 2012, doi: 10.1021/EF300403A.

[103] J. Aminian, C. Galletti, S. Shahhosseini, and L. Tognotti, “Numerical Investigation of a MILD Combustion Burner: Analysis of Mixing Field, Chemical Kinetics and Turbulence-Chemistry Interaction,” *Flow, Turbul. Combust. 2012 884*, vol. 88, no. 4, pp. 597–623, Feb. 2012, doi: 10.1007/S10494-012-9386-Z.

[104] A. M. Briones, S. K. Aggarwal, and V. R. Katta, “A numerical investigation of flame liftoff, stabilization, and blowout,” *Phys. Fluids*, vol. 18, no. 4, p. 043603, Apr. 2006, doi: 10.1063/1.2191851.

[105] M. Farokhi and M. Birouk, “Assessment of fractal/wrinkling theories for describing turbulent reacting fine structures under MILD combustion regimes,” *Combust. Sci. Technol.*, vol. 193, no. 10, pp. 1798–1825, 2021, doi: https://doi.org/10.1080/00102202.2020.1715963.

APPENDICES

APPENDIX A: Mesh Independency Analysis

A mesh independency analysis was conducted on the adopted grate-firing biomass furnace. At the initial stage, the generated grid was created following the previous studies conducted on the same furnace. A local increase in grid resolution has been applied in the vicinity of the bed and at the secondary and tertiary jet exit locations. Later, more refined grids were created, and multiple simulations were conducted. The axial temperature and velocity were compared for four cases of grid number (i.e., coarse-1 with 240888 elements, coarse-2 with 393583 elements, fine-1 with 508609 elements and fine-2 with 549409 elements), and the results showed no significant change in the species concentration predictions as well as velocity and temperature profile along the centerline with further grid refinement beyond grid fine-1. Thus, the fine-1 grid was selected for this study. The results are shown in Figure 12.

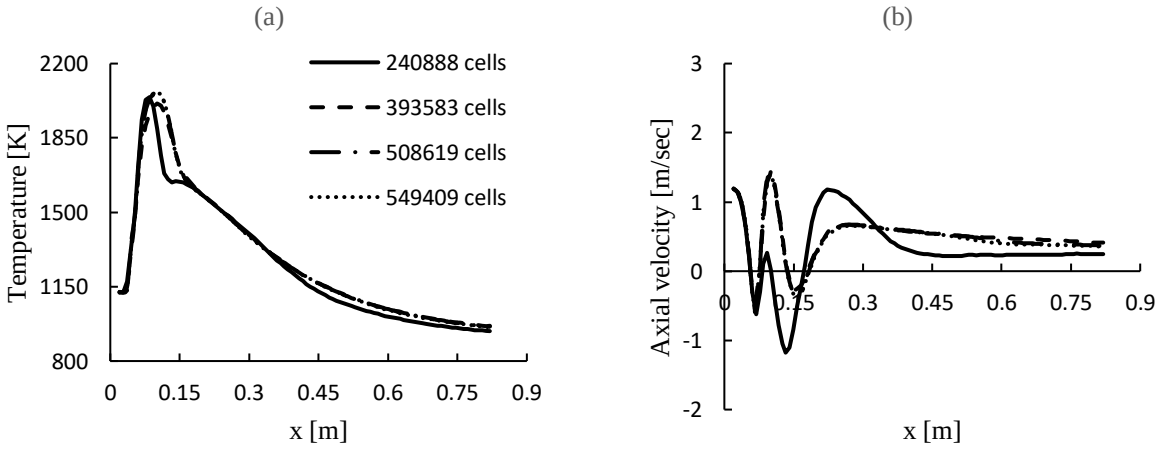

Figure 12. Numerical results of axial (a) temperature and (b) velocity along the centerline of the grate-firing biomass furnace using three different grids.

APPENDIX B: Scalar Dissipation Rate Analysis

In Chapter 5, downstream of the local high-temperature region (i.e., $x\sim > 0.3\,m$) has been described as chemical equilibrium region of the furnace. In order to conform this state, a scalar dissipation rate analysis was conducted. Scalar dissipation rate (χ_{st}) is the indicating factor that determines if a stoichiometric mixture is in a chemical equilibrium state or not [1]. According to the research conducted by Peters [2], chemical equilibrium of a stoichiometric mixture corresponds to the exact limit $\chi_{st} \to 0$. So as long as the value of χ_{st} is greater than 0, the stoichiometric mixture can not completely achieve a chemical equilibrium state. The result of the analysis is shown in Figure 13 and it clearly depicts that the scalar dissipation rate reaches 0, by the end of the high temperature region which signifies that the mixture attains chemical equilibrium state in that region.

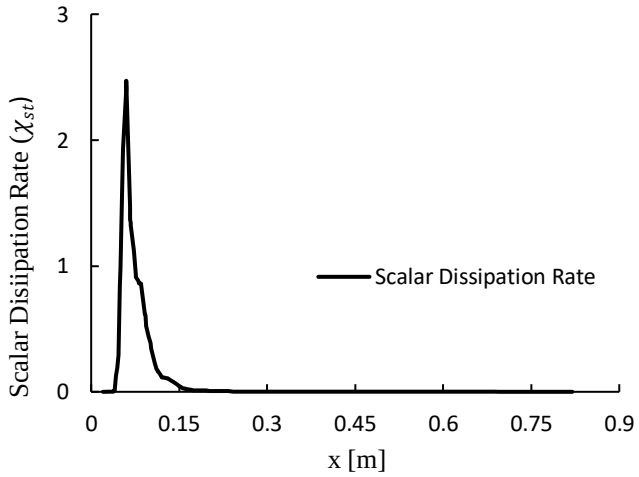

Figure 13: Numerical results of scalar dissipation rate along the centerline of the furnace.

B References

[1] H. Pitsch and H. Steiner, “Scalar mixing and dissipation rate in large-eddy simulations of non-premixed turbulent combustion,” *Proc. Combust. Inst.*, vol. 28, no. 1, pp. 41–49, 2000, doi: https://doi.org/10.1016/S0082-0784(00)80193-9.

[2] N. Peters, “Laminar diffusion flamelet models in non-premixed turbulent combustion,” *Prog. energy Combust. Sci.*, vol. 10, no. 3, pp. 319–339, 1984.